Can bioluminescence resonance energy transfer be used to elucidate structural and binding information about the ABCG2 transporter?

Joseph Morris

Thesis submitted to the University of Nottingham for the degree of Master of Research

COVID-19 impact

The COVID-19 pandemic caused significant disruption to this research project. The closure of the university and laboratory for six months, social distancing changes regarding attendance and lab capacity, and all the inconveniences that come with this have made carrying out an MRes very difficult. Some of the challenges have included remotely planning experiments, receiving socially-distanced equipment training and liaising with off-campus colleagues and supervisors. Added to this were two periods of contact isolation, one period suffering from COVID-19 itself, and the side effects of two vaccinations. Finally, there have been the wider impacts on the virus on society and my family which have made this an extraordinarily challenging time to undertake such a project.

Abstract

ATP binding cassette G2 (ABCG2) is a multidrug transporter involved in cancer cell resistance to chemotherapeutics. Uncovering ABCG2 structural and binding information and screening for potential inhibitors is crucial for increasing chemotherapy effectiveness and improving cancer prognoses. The present study examines the potential for bioluminescence resonance energy transfer (BRET) to report on ABCG2: substrate interactions, transporter conformation, and substrate specificity. Three NanoLuc-tagged mutant ABCG2 isoforms designed to alter substrate affinity and specificity were generated and expressed in HEK293T cells and membrane suspensions. NanoBRET assays were carried out in cells and membranes with a concentration range of fluorescent substrates mitoxantrone and rhodamine 123, sometimes in the presence of ABCG2 inhibitor Ko143 and a range of additives. NanoBRET successfully reported on binding of rhodamine 123 by ABCG2 through positive dose-response, however nonspecific BRET effects and/or low affinity substrates prevented the transporter from saturating. This bystander BRET effect appeared to mask differences between ABCG2 constructs, and the effect of Ko143. Therefore, further research with higher affinity ligands or substrates alongside more comparable control cell lines in parallel is required to fully evaluate BRET with ABCG2.

Acknowledgements

I'd like to thank Dr Ian Kerr and Dr James Mitchell-White as my supervisors, friends, and mentors who made this possible. I'm very grateful for all the advice and ideas you've helped me to develop, and the patience you've shown throughout this challenging project. Another big thank you to Deborah Briggs who spent many frustrated hours helping me get to grips with new equipment and techniques. Alongside this I'd like to thank all the other lab members who helped me along the way: Ella Hutchison, Dr Alistair Hume, Asmahan Alghamdi and Susie Entwistle. I wish you all the best of luck in your future endeavours.

With special thanks to Dr Joelle Goulding, Dr Laura Kilpatrick and Dr Mark Soave for guidance and training on everything BRET related, I couldn't have done it without you guys! I really appreciate all the time and effort you put into discussing my project and helping me with imaging and assays.

Declaration

This thesis, "Can bioluminescence resonance energy transfer be used to elucidate structural and binding information about the ABCG2 transporter?", is the result of my own work undertaken during my period of registration at the University of Nottingham under the supervision of Dr Ian Kerr. Technical assistance, and collaborations where relevant, have been acknowledged.

Abbreviations

ABC	ATP-binding cassette
ABCA	ATP-binding cassette family A
ABCB	ATP-binding cassette family B
ABCC	ATP-binding cassette family C
ABCD	ATP-binding cassette family D
ABCE	ATP-binding cassette family E
ABCF	ATP-binding cassette family F
ABCG	ATP-binding cassette family G
ADP	Adenosine diphosphate
ALD	Adrenoleukodystrophy
APS	Ammonium persulphate
ATP	Adenosine triphosphate
β_2AR	Beta-2-adrenergic receptor
BCRP	Breast cancer resistance protein
BRET	Bioluminescence resonance energy transfer
BSA	Bovine serum albumin
cDNA	Complementary DNA
CMV	Cytomegalovirus
DMEM	Dulbecco's modified Eagle's medium
DMSO	Dimethyl sulfoxide
E_1S	Estrone-1-sulfate
E211Q	Glutamate to glutamine substitution at position 211
ECL	Enhanced chemiluminescence
EM	Electron microscopy
F439A	Phenylalanine to Alanine substitution at position 439
FCS	Foetal calf serum
FLuc	Firefly luciferase
FRET	Fluorescence or Förster resonance energy transfer
FTC	Fumitremorgin C

GFP	Green fluorescent protein
GPCR	G-protein coupled receptor
HBSS	Hank’s balanced salt solution
HEK	Human embryonic kidney
LB	Luria-Bertoni
MATE	Multidrug and toxic compound extrusion
MalFGK2	E. coli maltose transporter
MCF-7	Michigan cancer foundation-7
MetNI	Methionine ABC Transporter
MDR	Multidrug resistance
MIB	Membrane isolation buffer
ModBC	Molybdate ABC transporter
MSU	Monosodium urate
MX	Mitoxantrone
NBD	Nucleotide binding domain
NLuc	NanoLuc
PBS	Phosphate buffered saline
PCR	Polymerase chain reaction
PEI	Polyethyleneimine
PhA	Pheophorbide A
Pi	Inorganic phosphate
P-gp	Permeability-glycoprotein
R123	Rhodamine-123
R482A	Arginine to alanine substitution at position 482
RET	Resonance energy transfer
SEM	Standard error of the mean
SDS	Sodium dodecyl sulphate
SDS-PAGE	Sodium dodecyl sulphate–polyacrylamide gel electrophoresis
SLC	Solute carrier family
SMALPs	Styrene maleic acid lipid particles

SNP	Single nucleotide polymorphism
SV40	Simian virus 40
TEMED	Tetramethyl ethylenediamine
TM	Transmembrane
TMD	Transmembrane domain
TNF-α	Tumour necrosis factor α
WT	Wild-type

Table of Contents

1.0 Introduction

1.1 Cell Membrane

Cell membranes form the barrier between the contents of the cell and the outside world. The current understanding of membrane structure is derived from that of the fluid mosaic model proposed almost half a century ago (Singer & Nicolson, 1972). This model suggests that the cell membrane consists of a bilayer of phospholipids to which proteins are bound, encapsulating a hydrophobic matrix. Many important biochemical processes occur at the cell membrane, mainly through a large selection of membrane-bound cellular enzymes. The fluid mosaic concept itself is based upon these two defining characteristics of the cell membrane. Firstly, the organisation of the phospholipids into a 'mosaic-like' structure depends upon the amphipathic nature of the lipids themselves, which results in spontaneous alignment of their hydrophilic heads and hydrophobic tails. Secondly, cell membranes exhibit a fluid-like property due to the constant rotational and translational movement of individual lipids and proteins within the membrane itself. Whilst cell membranes exhibit general symmetry in their structural appearance, the lipid components of the cell membranes themselves are inherently asymmetric due to a lack of trans-bilayer relocalisation (Goñi, 2014). Whilst movement between the two lipid layers forming the bilayer is theoretically possible, the high energy cost associated with performing a 'flip-flop' means this cannot occur spontaneously. However, flippases and floppases are P4-ATPases and ABC transporters which use adenosine triphosphate (ATP) to facilitate trans-bilayer diffusion to the cytosolic and exoplasmic faces respectively, helping to establish membrane asymmetry (Hankins et al., 2015). These factors mean many bilayers exhibit asymmetry in the lipids that form them; for instance, red blood cell inner membranes are composed almost entirely of phosphatidylserine lipids. The key characteristics of the fluid mosaic model of cell membranes can be seen in **figure 1.1.**

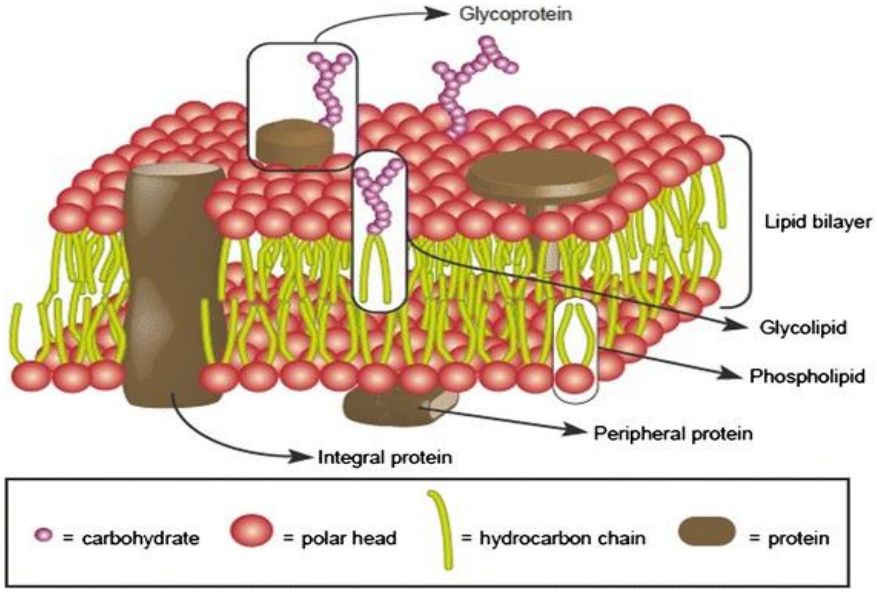

Figure 1.1. Fluid mosaic model of cell membranes. Phospholipid bilayer mosaic containing various proteins enclosing a hydrophobic matrix. Image received from Lombard, 2014.

1.2 Membrane transport

There are several different ways in which a chemical species may be transported across a membrane, and these mechanisms are generally categorised into two groups: active and passive transport. Whilst gases like oxygen may pass through a membrane by simple diffusion, larger or charged molecules must instead be transported across the membrane by a transport protein. These proteins can transport passively down a concentration gradient as is the case with many channels and carriers. However, if transporting against a concentration gradient then energy must be supplied, which is known as active transport. Therefore, many membrane transport proteins also exhibit ATPase activity in order to provide energy for these processes (Hediger et al., 2013). These ATP-linked transporters are designated primary active transporters as the ATPase activity is directly coupled to the transport process. On the other hand, secondary active transport does not use direct ATP coupling as an energy source, instead relying on the electrochemical potential of the membrane established by primary active transport (Wilkens, 2015). This mechanism is otherwise known as co-transport and can be further divided into symport under which both species are transported in the same direction, and antiport under which the two species are transported in opposite directions.

There are many different families of transporters which play countless different roles in mediating the movement of species across cell membranes. One example is that of the solute carrier (SLC) family of transporters which facilitate solute movement downhill with electrochemical gradient and against electrochemical gradient via secondary active transport coupling. This SLC family contains over 66 sub-families consisting of over 400 members responsible for transporting a hugely diverse range of inorganic ions as well as charged and uncharged organic molecules via both symport and antiport (Lin et al., 2015). The multidrug and toxic compound extrusion (MATE) transporters are a prominent family of membrane exporters responsible for the excretion of xenobiotic and metabolic organic cations in eukaryotes, bacteria and archaea. These transporters function exclusively as secondary active transport antiporters coupling sodium or proton uptake with drug efflux (Omote et al., 2006). However, the present study instead focusses on another family of membrane transporters responsible for ATP-coupled primary active transport. ATP binding cassette (ABC) transporters is the nomenclature given to a superfamily of primary active membrane transport proteins which use the binding and hydrolysis of ATP as an energy source to facilitate transport.

1.3 ABC Transporters

ATP binding cassettes use energy derived from the binding and hydrolysis of ATP in order to transport substrates across the plasma membrane. The ABC transporter field emerged from studies on bacterial nutrient uptake in the 1970s. In the 1980s the first genes coding for ABC transporters were cloned from *Escherichia coli* and *Salmonella typhimurium* bacteria. Alongside this, the gene encoding mammalian permeability glycoprotein (P-gp) was cloned in 1985 as a suspected contributor to multidrug resistance

(MDR; see section 1.6) in mutant Chinese hamster ovary cells (Juliano & Ling, 1976). Advances in cDNA sequencing technology resulted in the discovery of highly conserved regions within nucleotide-binding domains (NBDs) present in all ATP-binding transporters; now known as the Walker A and Walker B motifs (Walker et al., 1982). These conserved NBDs soon became the defining characteristic of a whole group of membrane transporters termed ABC transporters in 1990 (Hyde et al., 1990). ABC transporters were soon found to be expressed across many different cell types in which they exhibited a wide range of functionally diverse biochemical processes (Theodoulou & Kerr, 2015). There have been as many as 49 different types of ABC transporter identified in humans, classified into seven families: A, B, C, D, E, F and G. The broad functions of these subfamilies are explained further in **table 1.1**.

ABC transporter subfamily	Background	Transporter examples
A	Cholesterol transport, and resistance to anti-cancer and anti-viral agents.	A1-A13 e.g. • ABCA1 - a key regulator of cellular phospholipid and cholesterol homeostasis (Schmitz & Langmann, 2001). • ABCA2 - overexpressed in mitoxantrone-resistant small cell lung cancer cell lines (Boonstra et al., 2004).
B	Peptide transport (TAP1/TAP2, ABCB10) and MDR.	B1-B11 e.g. • ABCB1 (P-gp/MDR1) - the first discovered efflux transporter (Kathawala et al., 2015). • ABCB4 – upregulated in soft tissue carcinomas (Januchowski et al., 2013).
C	Chloride channel (CFTR), insulin secretion (SUR) and MDR	C1-C12 e.g. • ABCC1 (MRP1) – upregulated in primary ovarian cancer cells • ABCC10 + ABCC11 – increased expression significantly associated with overall survival of colorectal cancer patients (Krizkova et al., 2016).
D	Expressed exclusively in the peroxisome; fatty acid metabolism (Dean et al., 2001)	D1-D4 e.g. • ABCD1- implicated in x-linked adrenoleukodystrophy (ALD); neurodegeneration due to accumulation of fatty acids (Kemp et al., 2001).
E	Do not contain TMDs	E1 • ABCE1 involved in ribosome recycling in mRNA translation (Zhu et al., 2020).
F	Do not contain TMDs	F1-F3 • Family thought to be involved in inflammatory processes; ABCF genes upregulated by TNF- α (Vasiliou et al., 2009).
G	Sterol transport and MDR	G1, G2, G4, G5, G8 e.g. • ABCG1 macrophage cholesterol homeostasis • ABCG2 involved in MDR

Table 1.1. Human ABC transporter subfamilies. The seven currently identified subfamilies of ABC transporters: ABCA. ABCB, ABCD, ABCE, ABCF and ABCG, with key examples.

1.4 ABC Transporter Structure

Eukaryotic ABC transporters are usually characterised by an architecture of four domains, generally consisting of two NBDs and two transmembrane domains (TMDs) containing 6 transmembrane (TM) α-helices each (Robey et al, 2018). Some ABC families feature transporters with extra domains, which are often identified first in sequencing and confirmed later when the full structures become available. Despite this, the ABCE and ABCF families of proteins do not possess TMDs, instead consisting only of NBDs which means they have no clear function with regards to membrane transport and therefore will not be discussed further (Ford & Beis, 2019). The single-particle cryo-EM structure of ABCA1 elucidated the presence of large extracellular domains between α-helix 1 and 2 in each TMD, which holds true for many members of the ABCA family (Qian et al., 2017). The ABCB subfamily is the only to contain both full and 'half' ABC transporters. Half ABC transporters only have one NBD and TMD as opposed to two of each. One 'monomer' of half transporter may then form homo-dimers, hetero-dimers or oligomers to form the dimerised NBDs required to bind ATP.

Members of the ABCC subfamily are often referred to as multidrug resistant proteins (MRPs), which can be further divided into short and long MRPs. Short MRPs exhibit the typical ABC transporter structure consisting of two TMDs and two NBDs. Long MRPs however feature an extra TMD at the N-terminus comprising an additional five transmembrane α-helices. Sequences present in this extra TMD, coined MSD0, are crucial for both plasma membrane trafficking and transport function in these long MRPs (Chen & Tiwari, 2011). A unique ABCC transporter is that in which mutations are responsible for the development of cystic fibrosis, cystic fibrosis transmembrane conductance regulator (CFTR). Unusually, CFTR acts as an ATP-gated anion channel with ions leaking from the open conformation as opposed to a traditional ATP transporter. Also unlike other ABC transporters, NBD1 in CFTR is connected to TMD2 via a regulatory 'R domain' which becomes phosphorylated to allow the channel to open upon the binding of ATP (Sheppard & Welsh, 1999). Homology modelling on the ABCD family has suggested their overall structure to be similar to that of traditional ABCB and ABCC transporters. The complete structures and functions of ABCD transporters are yet to be identified, however these transporters have been proposed to be involved in the transport of fatty acid substrates in the peroxisomal compartment. Sequence analysis of the ABCG family of transporters had previously identified a uniquely inverted arrangement with the NBD preceding the TMD, which was also seen in the full structure of the ABCG5/G8 transporter complex (Lee et al., 2016). This inverted arrangement also exists in the sequences and structures of all other identified ABCG transporters, such as in the cryo-EM structure of the ABCG2 transporter shown here in **figure 1.2a** (Dawson & Locher, 2006). In fact, this structure somewhat resembles that of some bacterial ABC transporters in size and shape, namely MalFGK2, ModBC and MetNI. Similarly to certain members of the ABCB family, all members of the ABCG subfamily are half transporters.

For membrane associated ABC transporters, the dimerised NBDs are linked to the two transmembrane domains consisting of six α-helices each, which span the membrane to form the bilayer translocation

pathway. The motifs responsible for linking the TMDs and NBDs are coupling helices which channel the conformational change mechanism responsible for membrane transport upon ATP binding and hydrolysis. For example in ABCG2, the channelling of this conformational change is key to the movement of substrate between the two binding sites cavity one and cavity two. Cavity one is the first binding site for substrate before substrate transfers to cavity two upon conformational change and subsequent removal of the leucine plug previously blocking the pathway. Critical to the three-dimensional structure and function of all ABC transporters are the Walker A and Walker B motifs, which are highly conserved across all ABC families as well as across other eukaryotic and prokaryotic ATP and GTP binding proteins (Walker et al., 1982). In ABC transporters, the Walker A motif is found in close to the N-terminus of the NBD. The glycine-rich Walker A motif itself (also known as the P-loop) is preceded by a β-strand and followed by an α-helix. Located within the Walker A motif is the crucial lysine residue responsible for binding the gamma-phosphate, and the backbone nitrogen atoms of other residues responsible for binding the alpha and beta-phosphates of the nucleotide, which in the case of ABC transporters is believed to be ATP (Hanson & Whiteheart, 2005). The combination of this P-loop with the ABC signature motif (LSGGQ) present in the opposite NBD results in two molecules of ATP being bound between the NBD interface, as seen in **figure 1.2b**. The Walker B motif is found within the NBD downstream of Walker A. This particular motif contains an aspartic acid residue responsible for promoting nucleotide hydrolysis via an Mg^{2+} ion (Chiraniya et al., 2013). Also contained in the Walker B motif is a catalytic glutamate residue (E211 in ABCG2) which, in combination with water molecules, is vital for ATP hydrolysis and therefore transporter function. The mutation of E211 to Q211 in ABCG2 prevents ATP hydrolysis thereby locking the transporter in an ATP bound conformational state. This mutation allowed for the resolution of the transporter cryo-EM structure in this ATP-bound state which is shown in **figure 1.2b**.

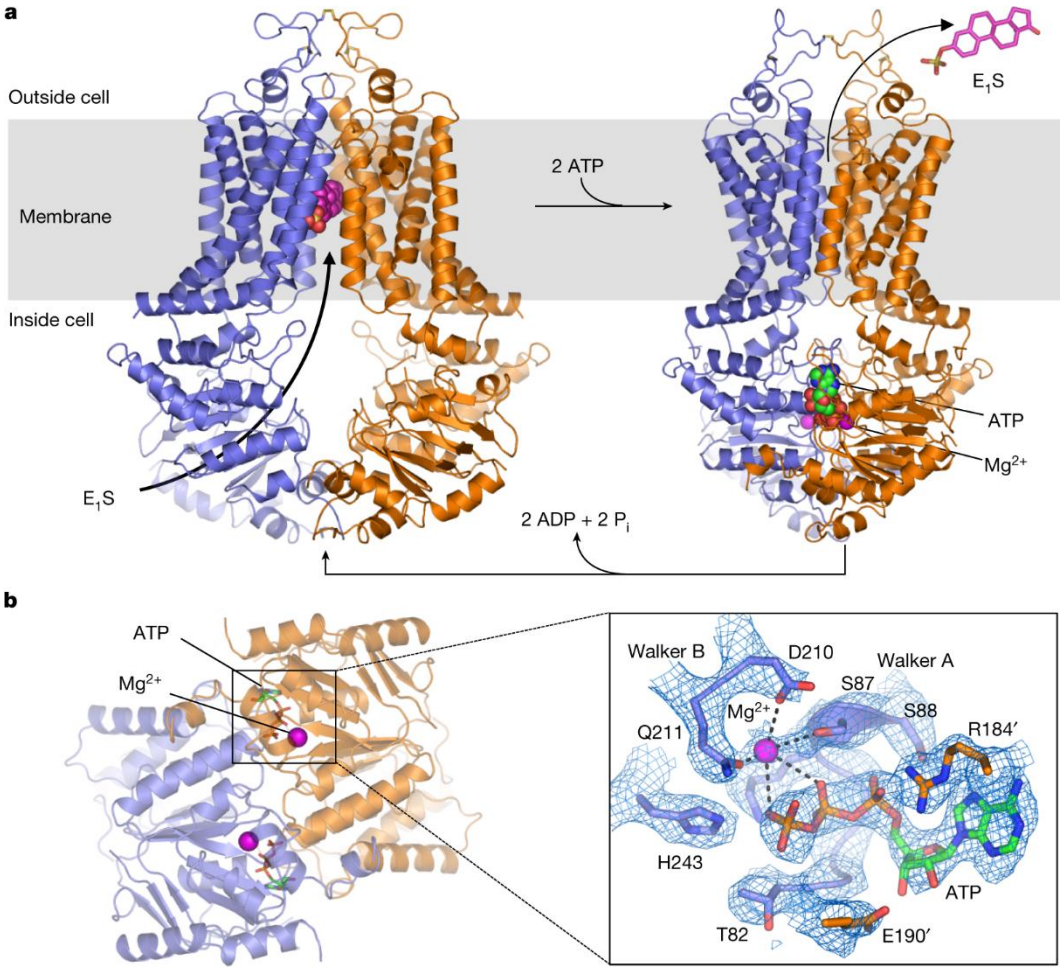

Figure 1.2. ABCG2 structure with A) substrate bound and B) ATP bound. Panel A shows the transporter switching between closed and open dimer conformations resulting in the extrusion of substrate and binding of and hydrolysis of ATP. Panel B shows two molecules of nucleotide sandwiched at the NBD: NBD interface with the key residues of the Walker A and B motifs in the E211Q ABCG2 mutant in which the transporter is locked in an ATP-bound conformation**.** Image taken from Jackson et al, 2018.

1.5 ABC Transporter Mechanism

The full mechanistic relationship between ABC transporter ATP coupling, ATP hydrolysis, substrate binding and subsequent related conformational change in the TMDs has been the subject of debate for decades. Many different theories and models have been proposed, but it is important to note that it is unlikely that all ABC transporters will operate via an identical mechanism. The three most favoured mechanisms are the alternating access, ATP switch and constant contact models for the ABC transporter catalytic cycle. Whilst these models all agree on the basic steps involved like NBD dimerization, the order and details of these steps vary. The ATP switch and constant contact models in particular are very close variations on the same mechanism under which transport is driven by NBD conformational switching, whilst the alternating access model couples this with TMD conformational switching. Additionally, the changing NBD occupancy by ATP and ADP is mirrored by changes in affinity for substrates as shown by pharmacological analysis of ABCG2 and P-gp (Martin et al., 1999, Clark et al., 2006).

The ATP switch model (seen here in **figure 1.3A**) theorised by Higgins and Linton in 2004 and the constant contact model (seen here in **figure 1.3B**) theorised by Jones and George in 2009 both suggest that the driving force of the transporter mechanism is the changing of the NBD dimer between two states dependent on the binding and hydrolysis of ATP and subsequent release of nucleotide (Higgins & Linton, 2004; P. M. Jones & George, 2009). These models diverge in the fact that the constant contact model suggests only one ATP binding site opens fully at any one time, allowing previous nucleotide release and a new ATP molecule to bind before closing again. Whilst this site is now closed, the alternate ATP binding site is primed to open for ATP hydrolysis and nucleotide release. This cycle continues in alternating fashion resulting in constant contact between the two NBDs in the dimer, hence the name. Alternatively, the ATP switch model instead suggests the NBDs exist in either a closed dimer in which both ATP molecules are sandwiched together or an open dimer following sequential ATP hydrolysis and nucleotide release in which there is no contact between the NBDs (20-30 Å apart). For substrate export, this switch from the closed to open state drives the forward translocation of substrate through the transporter whilst the reverse switch of open to closed states acts to reset the transporter for another cycle.

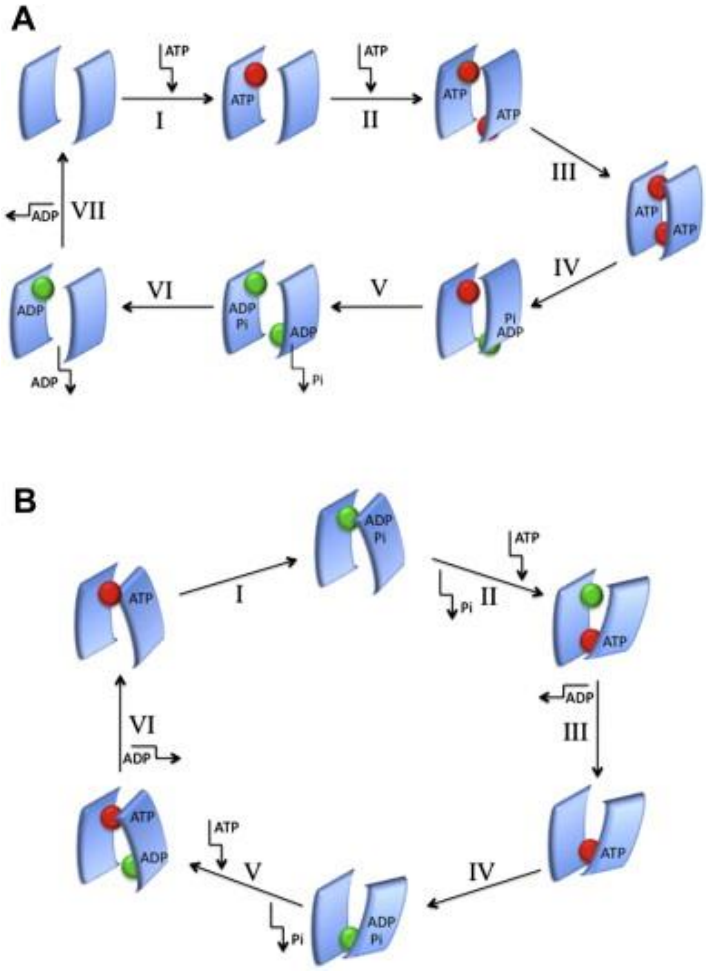

Figure 1.3. A) ATP switch model in which whole NBD dimers 'switch' between distinct open or closed conformations **and B) constant contact model** in which each ATP binding site of the NBD dimer opens sequentially resulting in constant NBD-NBD contact. NBDs are shown as blue bands and TMDs have been removed for simplicity. ATP is shown as red spheres and ADP as green. Image taken from George & Jones, 2012.

The alternating access model theorised by Dawson and Locher in 2006 suggests that both the NBDs and TMDs undergo conformational changes coupled to substrate and ATP binding and hydrolysis (Dawson & Locher, 2006). In this model, the ground state of the ABC transporter is known as the 'apo' state in which the TMDs are inward-facing. In this state ATP affinity is low with the NBDs in an open dimer configuration. This allows intracellular substrates to bind to the TMDs, inducing a conformational change in the NBDs. The effect of this conformational change acts to bring the NBDs closer together, thereby increasing binding affinity for ATP. Two ATP molecules bind co-operatively to the NBD dimer, changing its configuration to a closed state. This causes a conformational change in the TMDs which has the effect of opening a substrate binding cavity to the extracellular space from which the substrate is extruded as TMD substrate affinity lessens. Finally, the hydrolysis of the bound ATP molecules and subsequent release of Pi and ADP acts to restore the transporter back to its apo state. The proposed details of the alternating access model in the context of ABCG2 can be see here in **figure 1.4**. Panel 1 shows the binding of substrate topotecan, changing the conformational shape of the NBDs thereby allowing two molecules of ATP to bind. ABCG2 is now in a closed state as seen in panel 2, before the NBDs channel conformational change of the transporter into the outward-open state, removing the leucine plug between cavity one and two in panel 3. Substrate then passes from cavity one to cavity two and is extruded before the NBD dimer collapses in Panel 4, restoring the leucine plug. Finally, panel 5 shows the hydrolysis of ATP and subsequent release of ADP and Pi, restoring ABCG2 to its ground apo state for another cycle.

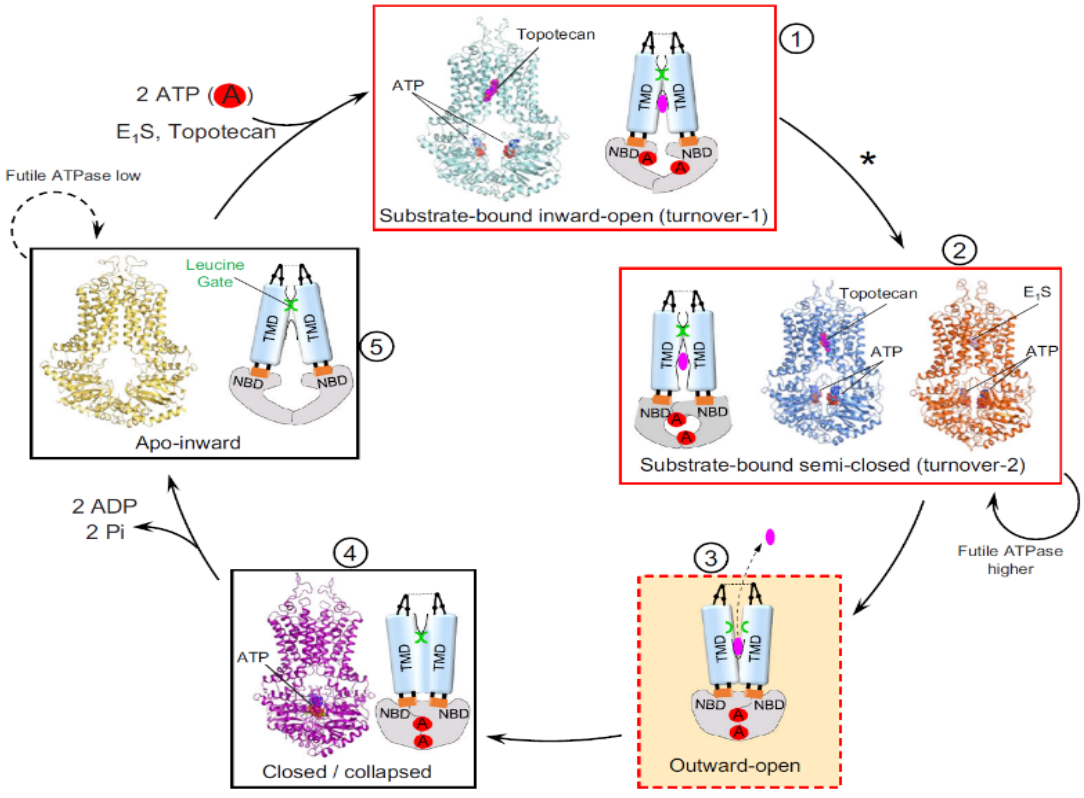

Figure 1.4. ABCG2 alternating access model. NBDs and TMDs both undergo conformational changes driven by binding of substrate topotecan, binding and hydrolysis of two ATP molecules and subsequent release of ADP and Pi (Lochers et al. 2021). Substrate is shown in purple, ATP is shown in red and leucine plug is shown in green.

1.6 ABC Transporters and Multidrug Resistance

Multidrug resistance in cancer cells is the phenomenon under which these cells have intrinsic, or otherwise acquire, resistance to multiple distinct chemotherapeutic agents. Primary multidrug resistance occurs in a relatively small proportion of malignant tumour cells or cancer stem cells which are 'naturally' resistant to chemotherapy drugs even from the beginning of treatment. Alternatively, secondary or acquired MDR is when surviving cancer cells develop resistance to multiple anticancer drugs even if they are not functionally or structurally related (Choi, 2005). This acquired resistance is particularly concerning for cancer prognosis, as it renders many forms of chemotherapy treatment ineffective.

Multiple studies have shown ABC transporters from most subfamilies to be involved in the efflux of many of these chemotherapeutic agents in many different cancers. As seen in **table 1.1**, some of the most infamous ABC transporters were initially named for the crucial role they play in MDR in tumours in which they are overexpressed (Choi & Yu, 2014). For example, the MDR1 (ABCB1) transporter is overexpressed in ovarian cancer cells and confers resistance to chemotherapeutics like paclitaxel and olaparid. These ovarian cancer cells were also found to be cross-resistant to several other anticancer drugs including doxorubicin and rucaparid (Vaidyanathan et al., 2016). It is also important to note that this MDR exhibited by ABCB1 can be reversed following treatment with ABC inhibitors such as verapamil or elacridar. The paper also confirmed the active efflux of all of these anticancer drugs both in the MDR ovarian cancer cells themselves as well as in ABCB1-expressing bacterial membranes. Therefore, research into the structure and pharmacological mechanisms behind the ABC transporters responsible for MDR is particularly clinically relevant in order to increase the effectiveness of chemotherapy treatment.

It has also become clear that tissues from a single tumour may express multiple different ABC transporters. In fact, studies examining expression of all 49 human ABC transporters in 281 samples of acute myeloid leukaemia (AML) have shown a demonstrable correlation between increased ABC transporter expression and decreased rates of survival (Marzac et al., 2011). More alarmingly, aside from the obvious candidates for MDR in AML like ABCB1, ABCC1 and ABCG2, other ABC transporters including ABCB6, ABCC13 and ABCG1 were also associated with poor prognosis. This is a concerning discovery which indicates that MDR might be more complex than previously considered, involving many more ABC transporters than just the well-established triumvirate of ABCB1, C1 and G2. This emphasises the potential crucial role ABC transporters have in facilitating MDR.

1.7 ABCG2 Transporter Background

In 1976, Juliano and Ling identified a 170 kDa glycoprotein which was associated with cancer cell resistance to chemotherapeutic agents (Juliano & Ling, 1976). Later, this transporter would come to be known as p-gp or MDR1; the first membrane protein to be implicated in MDR. Over 20 years later in 1998, Doyle et al. would clone another ABC transporter involved in drug efflux from the MCF7 breast cancer cell line, which they named breast cancer resistance protein (BCRP; Doyle et al., 1998). Soon after, Allikmets

et al would also clone a transporter from placental tissue differing in just one amino acid substitution at position 482, later identified as the wild type, which they would coin ABCP (Allikmets et al., 1998). A third group also cloned the same transporter as Doyle et al, but from a mitoxantrone-resistant colon cancer cell line S1-M1-80, which they named MXR (Miyake et al., 1999). When the full sequences of these proteins were identified, all three were found to be nearly identical 655 amino acid proteins with two differing in single amino acid substitutions. Critically, all of these cell lines showed MDR without expression of the previously identified MDR genes. The transporter was then renamed ABCG2 due to conserved homology with other ABCG family transporter sequences. Over the next decade many in vivo studies were carried out using ABCG2 knockout mice which showed the vital connection between ABCG2 and cellular efflux mechanisms associated with xenobiotic defence (Jonker et al., 2002).

1.8 ABCG2 Transporter Physiology

It is undoubtedly the case that the human ABCG2 transporter is vital in fulfilling multiple physiological roles in various different tissues throughout the body, demonstrated by high levels of expression in the brain, gastrointestinal (GI) tract, liver, and placenta. The most important of these roles is in the defence of cells and tissues from the damaging accumulation of cytotoxic substances, be that naturally occurring or xenobiotic in nature. The significance of ABCG2 is perhaps highlighted most effectively by its expression in the blood-brain-barrier where the transporter is vital in preventing toxic molecules from reaching the brain (Eisenblätter et al., 2003). Interestingly, this mechanism of drug efflux exhibited by ABCG2 is also critical to the nutritional composition of breast milk, namely with studies finding ABCG2 transporters expressed in the mammary gland to be responsible for concentrating riboflavin into milk during lactation. Indeed, it would seem this is conserved across most mammals including mice in which ABCG2 knockouts showed a 60-fold reduction in riboflavin milk secretion (van Herwaarden et al., 2007). This may suggest that the powerful mechanism of drug transport facilitated by ABCG2 could have been harnessed by evolution for use in transporting other crucial nutrients, vitamins or drugs into beneficial locations.

One of the main functions of ABCG2 in the gut and kidney is as an oxypurinol and urate transporter. However, the most common single nucleotide polymorphism (SNP) of the transporter, Q141K, consists of a glutamine to lysine substitution which prevents effective protein processing and trafficking via destabilisation of the NBD (Woodward et al., 2013). This results in decreased ABCG2 membrane expression and subsequent reduction of renal urate excretion by over 50%. Consequently, urate may begin to accumulate within the renal system forming monosodium urate (MSU) crystals which may be further deposited into articular structures surrounding synovial joints. The deposition of these MSU crystals can then induce an inflammatory immune response in synovial tissue leading to arthritis, or more specifically, gout. To exacerbate the problem, the Q141K polymorphism is also associated with a poor therapeutic response to the primary pharmaceutical treatment for gout, allopurinol, a xanthine oxidase inhibitor (Wrigley et al., 2020).

1.9 ABCG2 Transporter Topology and Oligomerisation

As previously stated, the G family of ABC transporters is unique in that they are membrane-bound reverse half transporters. They consist of just a singular NBD and TMD in an inverted arrangement of NBD preceding TMD unlike other ABC families which instead have two of each domain (excluding the peroxisomal ABCD1 which also dimerises) in the standard arrangement. Therefore, in order to function correctly, ABCG2 must dimerise or even form higher-order oligomers (Wong et al., 2016). Without two functional NBDs, ATPase activity and therefore substrate transport cannot take place. In fact, it may be the case that ATP binding and hydrolysis is key to inducing this homodimer coupling in ABCG2 monomers. That said, this concept is not unusual as there are several other examples of similar transport proteins which too dimerise, including TAP1 and TAP2 involved in the MHCCI pathway, and of course other ABCG transporters like ABCG8 and ABCG5 (Li et al., 1997). Interestingly, ABCG5 and ABCG8 can form a functional heterodimeric transporter, ABCG5/G8 (Yu et al., 2014). As for higher order oligomers, research has shown ABCG2 to not only form tetramers, but has in fact shown the potential of a predominantly tetrameric transient complex stoichiometry for ABCG2. However, the mechanisms by which these tetrameric ACBG2 complexes may form, and the effect this has on the activity of the transporter are yet to be uncovered.

1.10 ABCG2 Transporter Substrates

As a multidrug transporter, ABCG2 has many transportable substrates. These substrates include several classes of anticancer drugs such as anthracyclines, topoisomerase inhibitors and camptothecin analogues. Alongside this, other drugs like pheophorbide A (PhA), antimetabolites and glucuronide conjugates are also transported by ABCG2, as well as more general xenobiotic compounds (Mo & Zhang, 2012). Some significant examples of ABCG2 substrates are summarised in **table 1.2**. One study also implicated up-regulated ABCG2 transporters in the cerebrovascular deposition of amyloid beta peptide plaques; the build-up of which may be a contributory factor to the onset of Alzheimer's disease (Xiong et al., 2009). There are also differences in substrate specificity between mutant isoforms of ABCG2, for example wild type ABCG2 cannot transport the chemotherapeutic anthracycline doxorubicin but the R482A mutant can, as it has a much higher affinity for this substrate. Crucially, this diverse range of substrates share no underlying fundamental chemistry which could explain their transport by ABCG2.

ABCG2 Substrates	
Drug class	Substrate example
Anthracyclines	Idarubicin (Abbott et al., 2002)
Topoisomerase inhibitors	Mitoxantrone (Brangi et al., 1999)
Camptothecin analogues	Topotecan (Yang et al., 2000)
Antimetabolites	5-fluorouacil (Mo & Zhang, 2012)
Sulfated conjugates	Estrone-3-sulfate (E_1S, Imai et al., 2003)
Antibiotics	Erythromycin (Robey et al., 2009)

Anti-inflammatories	Diclofenac (Lagas et al., 2009)
Antivirals	Abacavir (Pan et al., 2007)
Polyglutamates	Methotrexate (Volk & Schneider, 2003)

Table 1.2. Drug class and examples of ABCG2 substrates.

1.11 ABCG2 Transporter Inhibitors

The mechanisms behind inhibition of the ABCG2 transporter are not yet fully understood but it is likely the case that many inhibitors act competitively and bind to ABCG2 akin to substrates (Toyoda et al., 2019). However, there is growing evidence that many inhibitory molecules bind to cavity 1 within the TMDs where they remain instead of transferring to cavity two, thereby locking the ABCG2 in in an inward conformation and preventing substrate transport. This is demonstrated by the large reduction in size of cavity one between the turnover-1 (~1300 Å) and turnover-2 (~830 Å) states seen in **figure 1.4** and more closely in **figure 1.5**, which results in considerable steric clashes with bound inhibitory Ko143 derivatives MB136 and MZ29 (Qin et al., 2021). Some research suggests that inhibitors may form more numerous contacts with the amino acid residues present in cavity 1 itself, which would explain why many inhibitors show a greatly increased binding affinity for G2 compared to substrates (Inhibitor Ko143 exhibits a 3000-fold increase in binding affinity compared to substrate E_1S, Jackson et al., 2018). With this being the case, it is probable that an inhibitor would not be able to move to cavity 2 as a substrate would, meaning cavity 1 cannot be closed and subsequent conformational change into an outward-facing cannot take place. Therefore, these conventional inhibitors act competitively through the physical blocking of cavity 1, and subsequent locking of ABCG2 into this inward-facing state preventing the transport cycle from advancing.

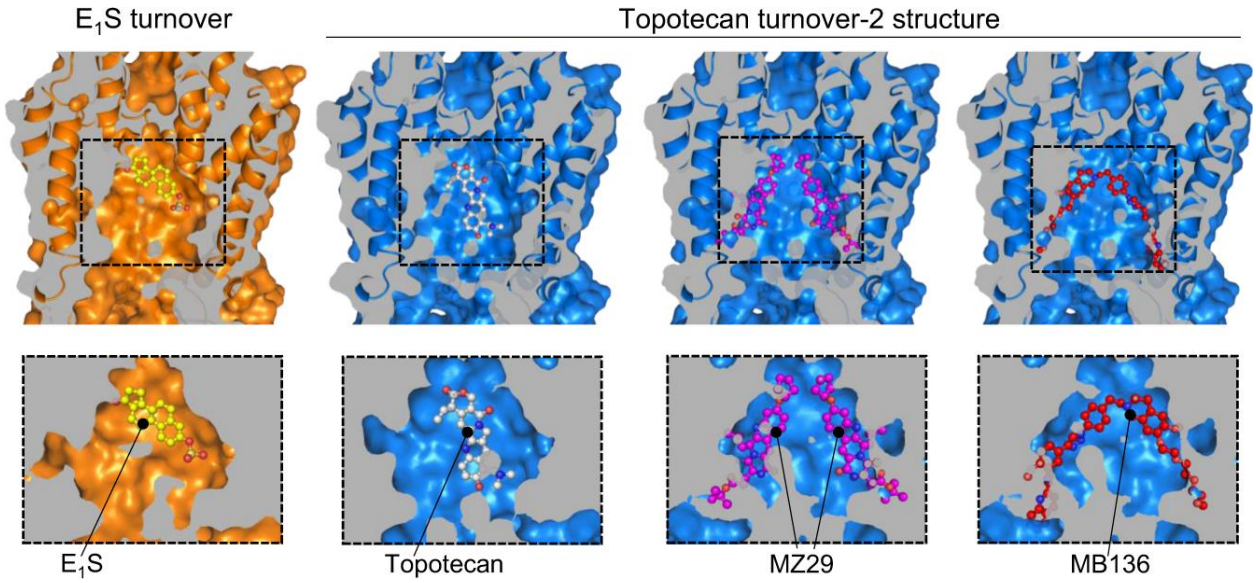

Figure 1.5. ABCG2 Turnover-2 structures demonstrate steric clashes with inhibitors. The four panels show substrates E_1S and topotecan and inhibitors MZ29 and MB136 bound within cavity one of the ABCG2 transporter. The substrates fit within the cavity whereas the inhibitors introduce steric clashes with the binding site. These steric clashes inhibit ABCG2 by preventing the transport cycle from advancing and locking the transporter in an inward-facing state. Bound inhibitors MZ29 and MB136 cannot translocate from cavity one to cavity two, whereas E1S and topotecan undergo usual transport. Image taken from Qin et al., 2021.

Interestingly, cavity 1 has a strong conformational rigidity regardless of the specific ligand bound and can distinguish between inhibitors and substrates when ATP is bound despite the shape of the cavity being conserved. This is demonstrated through the binding of cholesterol (as an analogue of substrate E_1S) under which ATPase activity was fully active versus the binding of inhibitor MZ29 in which ATPase activity was abolished (Jackson et al., 2018). It is also the case that two inhibitory molecules can be bound within the cavity at the same time, but whether this extends to substrates to allow for the transport of two molecules simultaneously is unknown. As with much of ABCG2, the unknown details behind these mechanisms have slowed the pharmaceutical development of ABCG2 inhibitors, none of which have been deemed safe and effective enough to gain approval for clinical use. Developing an effective ABCG2 inhibitor could be crucial as part of a combination drug therapy to increase the efficacy of anticancer treatment through inhibition of ABCG2-mediated chemotherapeutic efflux (see **section 1.12**). One of the most widely studied ABCG2 inhibitors is a derivative of an *Aspergillus fumigatus* mycotoxin (FTC), called Ko143. Ko143 has been found to be a very potent inhibitor of the transporter, however the molecule is yet to make it past in vivo pre-clinical testing (Mairinger et al., 2018). Some of the drugs that have been identified as inhibitors of ABCG2 are summarised in **table 1.3**.

ABCG2 Inhibitors	
Drug class	Substrate example
Immunosuppressants	Cyclosporin A (Gupta et al., 2006)
Tyrosine kinase inhibitors	Imatinib (Houghton et al., 2004)
Calcium channel antagonists	Nicardipine (Shukla et al., 2005)
Antifungals	Fumitremorgin C (FTC, Rabindran et al., 1998)
Protease inhibitors	Ritonavir (Gupta et al., 2004)
Synthetics	Ko143 (FTC derivative, Allen et al., 2002)

Table 1.3. Drug class and examples of ABCG2 inhibitors.

1.12 ABCG2 Transporter and Multidrug Resistance

The long list of potent anti-cancer drugs identified as substrates for ABCG2 illustrates the important role of this transporter in facilitating multidrug efflux. As with many other ABC transporters, the primary method of acquired MDR seems to be a result of overexpression as opposed to specific mutations to ABCG2. That being said, it was the mutations to the ABCG2 transporter responsible for the MDR phenotype observed in the original breast cancer cell lines, as opposed to just the presence of ABCG2 itself. Genomic analyses of ABC transporter mRNA expression have identified a fundamental link between cancers traditionally resistant to chemotherapy like nephrocytic or hepatocytic and high levels of ABCG2 and ABCB1 expression. These cancers are frequently resistant to chemotherapeutics like doxorubicin and vincristine which are natural substrates for both ABCG2 and ABCB1 (Robey et al., 2018). ABCG2 is also expressed in haematopoietic stem cells, and studies have implicated the transporter in providing chemotherapy resistance in AML. In fact, overexpression of ABCG2 at AML diagnosis is indicative of particularly poor disease prognosis even after treatment with allogenic stem cell transplantation (Damiani

et al., 2015). Therefore, the effect of ABC transporters and more specifically ABCG2 itself on the development of MDR is clear to see.

1.13 Pharmacology of ABCG2

There have been many studies into the pharmacology of ABCG2 to try and better understand the specific interactions between the transporter and its substrates. These studies have revealed key details like the existence of at least two parallel substrate binding sites on ABCG2, which indicates the ability of ABCG2 to interact with multiple substrates simultaneously (Clark et al., 2006). Another example is the identification of the roles played by ATP and substrate within the transport mechanism, more specifically the fact that binding of ATP displaces that of substrate which is indicative of low ABCG2 affinity for substrate when ATP is bound. This suggests that the dissociation of ATP is responsible for restoring the transporter to its ground state to again allow substrate to bind (McDevitt et al., 2008). Many of these previous studies have used radiolabelled ligands to precisely interrogate these interactions in cells and membranes, which have high sensitivity but can be expensive or dangerous to work with. Therefore the development of equally effective alternative assay techniques could be beneficial in enabling the continued research into the better understanding of the pharmacology of ABCG2 and its substrates.

1.14 Bioluminescence Resonance Energy Transfer

Resonance energy transfer (RET) is an optical phenomenon under which energy is transferred from an energetic donor to an acceptor molecule via dipole-dipole interactions. This transfer of energy is found in nature where photosynthetic plants and bacteria harness this mechanism to transfer and focus energy absorbed by photosynthetic pigments toward the centre of the light-harvesting complex (Olejko & Bald, 2017). The development of this concept in the late 1920s is credited to Theodore Förster who theorised that this energy transfer depended upon two key aspects of the molecules involved, intermolecular distance and spectral overlap (Jones & Bradshaw, 2019). We now know that the ideal range between the donor and acceptor molecules for facilitating effective RET is under 10 nm, and if optical spectra do not overlap then RET cannot take place between two molecules. However, if a suitable pair of molecules with sufficiently overlapping spectra can be identified, then this donor and acceptor can be used to tag two species of interest thereby reporting on the interactions of these two proteins.

Fluorescence resonance energy transfer (FRET) was the first developmental iteration of this natural RET mechanism in which exogenous fluorescence excitation would be applied to the fluorescent donor molecule in order to facilitate RET. Whilst this was a successful technique for studying protein interactions, the external fluorescent excitation introduced background noise to the reading and made it difficult to study intracellular interactions in live cells. Therefore, scientists again looked to nature to identify and develop a new iteration of RET technology. Bioluminescence resonance energy transfer instead uses a bioluminescent enzyme as the donor molecule. Fluorescent excitation is not required; instead BRET uses the addition of a chemical substrate for this bioluminescent enzyme resulting in bright

bioluminescence. This phenomenon is seen in various deep-sea marine species which use bioluminescence both to find prey and avoid predators. The main advantages of BRET over FRET include the removal of several detrimental effects like background noise, autofluorescence, light scattering and photobleaching, alongside being much easier to use in the imaging of interactions in live species. The current most common use of this technique is found in the study of G-protein coupled receptors (GPCRs) in which BRET allows for the activity of receptor-coupled downstream signalling complexes to be examined (Kobayashi et al., 2019). The mechanism by which BRET takes place is shown in **figure 1.6**.

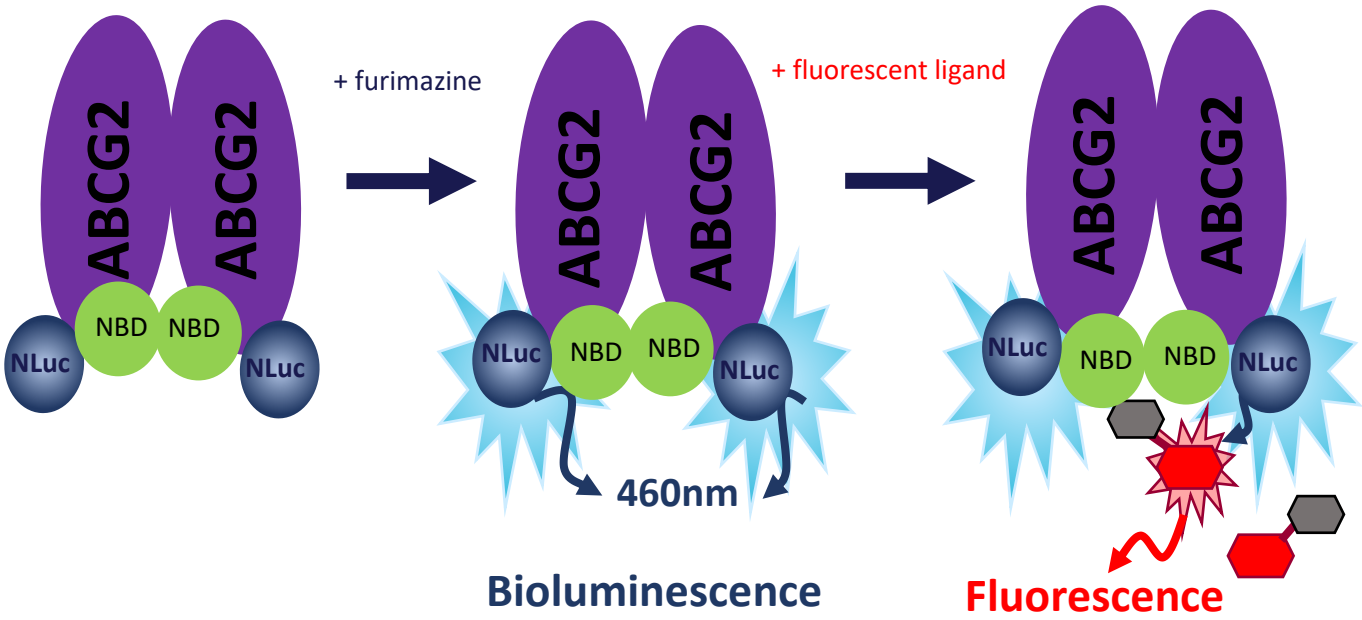

Figure 1.6. Mechanism of BRET. Diagram showing the mechanism by which BRET occurs from bioluminescent transporter to fluorescent acceptor. ABCG2 transporters are N-terminally tagged with NanoLuc luciferase which exhibits bioluminescence when exposed to its substrate furimazine. If fluorescent drug comes within 10 nm of bioluminescent transporter, then resonance energy transfers from donor (transporter) to acceptor (drug). The ratio of fluorescence to bioluminescence can be measured as a quantitative measurement of binding activity.

1.15 NanoLuc luciferase

The specific luciferase enzyme chosen for this research is NanoLuc (NLuc) for use in NanoBRET-based assays. The NLuc enzyme is a novel 19.1 kDa luciferase derived from deep-sea shrimp. The enzyme functions through converting a coelenterazine substrate analogue, furimazine (2-furanylmethyl-deoxy-coelenterazine) into furimamide which exhibits a high intensity luminescence at 460 nm. An emission spectrum for NLuc can be seen later in **figure 3.9**. A fluorescent drug bound to ABCG2 tagged at the N-terminus with NLuc should exhibit BRET upon the addition of furimazine, resulting in a characteristic fluorescence emission at the expected wavelength which can be measured. The ratio of fluorescence exhibited by the drug divided by the bioluminescence exhibited by the NLuc enzyme is known as the BRET ratio or signal. This provides a quantitative reading of binding ABCG2 by a fluorescent drug. The two fluorescent drugs used in this study are mitoxantrone (MX) and rhodamine 123 (R123) with excitation

peaks of 610 nm and 508 nm respectively. Furthermore, the increased brightness of this luciferase allows for effective monitoring of cell surface localisation of tagged proteins when examining cells under a bioluminescence microscope. This means that cell populations can be checked for the appropriate trafficking of the ABCG2 transporter to the cell surface, as well as being used to verify successful transfection of cells with NLuc, potentially lessening the need for verification via other time-consuming techniques.

NLuc itself exhibits several preferred properties compared to other traditional luciferases like firefly luciferase (FLuc) derived from the North American Firefly. These benefits include increased thermal and pH stability, increased brightness and lower molecular weight when compared to FLuc which has a weight of 61.5 kDa. Utilising a smaller donor molecule is important to reduce the potential for unwanted steric effects when studying receptor: ligand interactions. These factors mean that NLuc is a more efficient and effective luciferase to use in the live imaging of cells at concentrations more physiologically relevant to the study. Furthermore, the stronger signal generated by NLuc enables the use of more red-shifted fluorescent acceptors, which can reduce emission spectra overlap between donor and acceptor, therefore improving signal-to-noise ratio (England et al., 2016).

1.16 Project objectives and hypothesis

Previous studies have investigated the effects of specific ABCG2 mutations on substrate binding and ATPase activity. The E211Q mutation consisting of a glutamate (E) to glutamine (Q) substitution at position 211 in the Walker B motif ablates the ATPase activity of the transporter, thereby preventing the transport of substrate. Theoretically, this mutation should lock the transporter in a conformational state with a greatly decreased affinity for substrate binding (McDevitt et al., 2009). Therefore, by using BRET to report on the binding activity of the E211Q mutant, we hope to test whether this imaging technology can effectively differentiate between ABCG2 isoforms with different degrees and activity of binding.

The R482A mutation consisting of an arginine (R) to alanine (A) substitution at position 482 in TM3 has been implicated in altering ABCG2 substrate specificity. R482A isoforms are able to transport substrates that WT ABCG2 cannot, including many chemotherapeutic drugs such as doxorubicin, mitoxantrone and rhodamine 123 frequently used in breast cancer treatment (Pozza et al., 2006). Therefore, there is potential for the use of BRET to elucidate crucial information regarding the location and mechanism of drug binding activity both in WT and mutant ABCG2 transporters. As much of these mechanisms are unknown, we hope to use BRET to provide quantitative measurements of binding activity which may be used to uncover more information about the transporter.

Recently, the specific role of R482 in altering the substrate specificity of ABCG2 has been investigated further. Past research suggested that mutations in R482 act on ATP hydrolysis and substrate transport, as opposed to preventing substrate binding (Ejendal et al., 2006). The R482 residue itself does not directly contact substrate as it is located in TM3, instead acting allosterically via contact with residue F439

in TM2. F439 channels conformational change in the TMDs via interactions with substrates bound in cavity one of the transporter (Taylor et al., 2017). In fact, the side chains of R482 interact with both side and main chain atoms in the vicinity of the F439 residue forming and breaking hydrogen bonds as the ABCG2 transporter moves through its alternating access transport mechanism. This seems to explain why interactions induced by the R482 residue are key to ABCG2 substrate specificity, and why single point mutations of this residue can have such a large impact via its action on F439 and subsequently the conformation of TMD2 as a whole (Lochers et al., 2021). Ko143 is a high affinity inhibitor of ABCG2 (see **section 1.11**), which is believed to bind to the same site as substrates. Therefore, by including Ko143 in these assays, any BRET signal should, in theory, be displaced as substrate could no longer bind.

By examining the potential of BRET to measure these key characteristics of the ABCG2 transporter like binding activity, we reach the final goal and clinical relevance of the project. If by using BRET to report on the activity of ABCG2 we achieve distinguishable BRET signals for the WT and mutant isoforms, this demonstrates that BRET may be used as a screening tool for potential chemotherapy drugs. In fact, the FDA guidelines state all new drugs of any kind have to be tested for ABCG2 activity, so the development of an effective BRET assay could assist with drug discovery and development (Giacomini et al., 2010). Hopefully, this technology can provide information about the interactions of drugs with WT and mutant ABCG2, thereby providing a system in which novel drugs could be examined to predict their specific transporter mechanics and activity. Furthermore, the information gathered from these interactions could be used to improve the design of potential future chemotherapeutic drugs, either as inhibitors for the ABCG2 transporter or more simply, just as drugs unable to be exported by ABCG2.

Therefore, the hypothesis of this project is three-fold. Firstly, BRET should be able to report on ABCG2: substrate interactions with a positive correlation between substrate concentration and BRET ratio in cells and membranes. Secondly, there should be a difference in BRET ratios between the four ABCG2 constructs (WT, R482A, E211Q and R482A/E211Q) indicative of altered substrate affinity and specificity. Finally, the ABCG2 inhibitor Ko143 should act to displace any BRET ratio through competitive binding with a much higher affinity for ABCG2. BRET should report on both transporter conformation and substrate specificity.

2.0 Methods

2.1 Molecular Biology

2.1.1 Primers

Predesigned forward and reverse primers (Sigma-Aldrich) incorporating both the R482A and E211Q mutations were used to generate mutant pc3.1 Zeo-NLuc-ABCG2 plasmids from WT plasmids (Kerr Lab, University of Nottingham). These primers, shown in **table 2.1**, are designed to insert the two mutations

into the WT ABCG2 cDNA present in the template vector. This plasmid also included the NLuc luciferase as well as Zeocin resistance. A map of the complete plasmid can be seen in **figure 2.1**.

Mutant	Forward primer	Reverse primer
R482A	5′-GATTTATTACCCATG**GCG**ATGTTACC-3′	5-GGTAACAT**CGC**CATGGGTAATAAATC-3′
E211Q	5′-ATCTTGTTCTTGGAT**CAA**CCTACAACAGGCTTAGACTCAAG-3′	5′-CTTGAGTCTAAGCCTGTTGTAG**GTT**GATCCAAGAACAAGAT-3′

Table 2.1. Primers used for ABCG2 mutations. Pre-designed primers for both R482A and E211Q mutations were obtained from Sigma Aldrich. Primers are given in the 5'-3' direction and mutated sequences are underlined in bold.

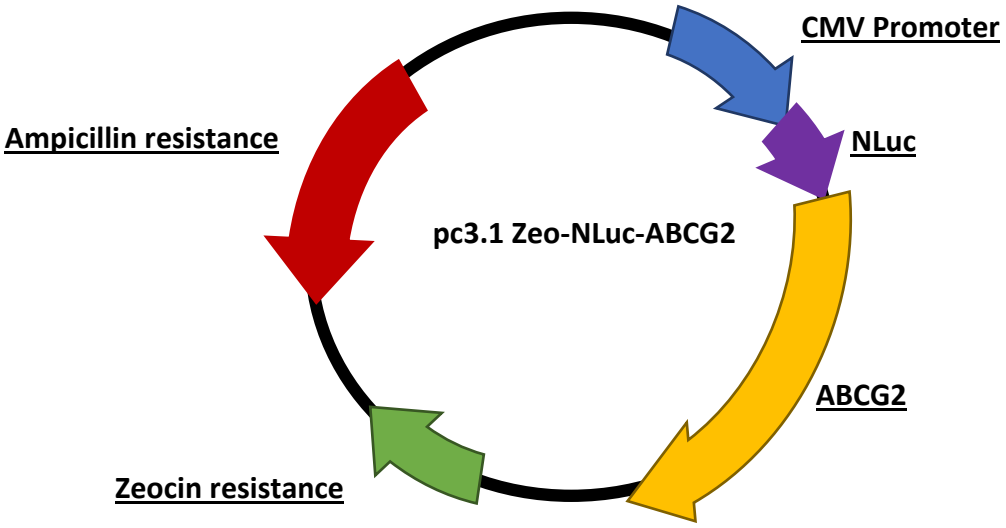

Figure 2.1. Map of the pc3.1 Zeo-NLuc-ABCG2 plasmid. Plasmid contains ABCG2 gene tagged with NanoLuc at the N-terminus as well as a CMV promoter region for high level transcription and Zeocin and ampicillin resistance genes for selection in mammalian and bacterial cells respectively. Plasmid length is ~8.1 kb. WT plasmid obtained from Kerr Lab, University of Nottingham.

2.1.2 Site-directed mutagenesis

The mutant isoforms of pc3.1 Zeo-NLuc-ABCG2 were generated through a Quikchange site-directed mutagenesis protocol in a Sensoquest Labcycler (Göttingen, Germany) polymerase chain reaction (PCR) unit. A typical PCR reaction mix of 50 µL consisted of 1X reaction buffer diluted from the manufacturers 10X stock; 1 µM each of forward and reverse primer; 200 µM of each dNTP; 50 ng of template DNA; 2-3 units of Pfu polymerase and finally ddH_2O to a final volume of 50 µL in thin-walled PCR tubes. The PCR program consisted of an initial denaturation step at 95˚C for 60 s followed by 16 cycles of amplification consisting of denaturation at 95˚C for 60 s, annealing at 55˚C for 60 s and extension at 72˚C for 12 minutes before a final extension period at 72˚C for 10 minutes. After the program had finished the samples were held at 10˚C, sometimes overnight. Following PCR, the methylated parental DNA was digested using DpnI. A typical digest would consist of 5 units of DpnI added to the PCR products before incubation for 30-60 minutes at 37˚C. After digestion, 5 µL of each PCR product was added to 15 µL ddH_2O and 4 µL 6X loading dye (40% w/v sucrose and 0.25% bromophenol blue) before electrophoresis. The double mutant isoform (R482A/E211Q) was generated through this same method except the

template DNA was replaced with the verified R482A mutant plasmid alongside the E211Q primers. This introduced the E211Q mutation into a sample of the plasmid already containing the R482A mutation.

2.1.3 Agarose gel electrophoresis

Agarose gel electrophoreses were carried out using a 1% w/v agarose gel containing 1 µg/µL ethidium bromide alongside a 1 kb DNA ladder (New England Biolabs; NEB). The buffer used was 1X TBE consisting of 90 mM boric acid, 90 mM Tris and 2 mM EDTA at pH 8.0. This is the standard agarose gel formulation and protocol used throughout the study unless stated otherwise.

2.1.4 Transformation

DH5-α competent *E. coli* cells were thawed on ice before 95 µL of DH5-α cells were added to chilled Eppendorf tubes for each transformation. 5 µL of the DpnI digest products were added to the respective DH5-α cells before they were incubated on ice for 30 minutes. Following this, the cells were then heat-shocked at 42˚C for 30 seconds before being placed back on ice for 5 minutes. Subsequently, 950 µL of Luria-Bertoni (LB, 10.0 g/L NaCl, 10.0 g/L tryptone, 5.0 g/L yeast extract) was added to each mixture to a final volume of 1000 µL. These tubes were then incubated in a shaker incubator at 200 rpm for ~60 minutes. Finally, the whole mixture was then plated on LB-agar-ampicillin plates (15.0 g/L agar and 100 µg/mL ampicillin) overnight at 37˚C. After incubation, individual colonies present on the plates were transferred into a 30 mL Sterilin tube containing 100 µg/mL ampicillin and 5 mL LB. These tubes were then incubated in an orbital shaker at 200 rpm overnight. The following day, 500 µL of the culture mixture was added to 500 µL 30% w/v glycerol to produce a glycerol stock of each culture to be stored at -80˚C. The remaining volumes of each culture were spun down at 4000 rpm (Eppendorf 5810 centrifuge) with the supernatant being discarded and the bacterial pellet retained.

2.1.5 Plasmid purification

This plasmid DNA was then extracted from the bacterial pellets by use of the Nucleospin plasmid kit from Macharey-Nagel through the alkaline lysis method. The final purified plasmid DNA was eluted in 30 µL of manufacturer's elution buffer and frozen at -20˚C ready for further use. A Nanodrop 2000 (Thermo Scientific, Labtech International) unit was used to measure the concentration of the plasmid DNA, as well as to assess the purity via the A260/A280 ratio. Generally, DNA samples were considered sufficiently pure with an A260/A280 ratio of between 1.7 and 2.0.

2.1.6 PvuII digest and DNA visualisation

A small quantity of purified plasmid DNA was digested with a restriction enzyme, PvuII, in order to validate the digested length of the plasmid. A total reaction mix of 20 µL containing 2 µL of NEBuffer 3.1 buffer, 1 µL of DNA, 1 µL of PvuII and 16 µL of ddH_2O was incubated at 37˚C for 60 minutes. Following this, 6X loading dye was added to the products before they were electrophoresed on an agarose gel as

discussed in section 2.1.3. The resulting bands were then visualised using a Syngene GENE bioimaging systems transilluminator compared to the 1kb DNA ladder.

2.1.7 DNA sequencing

The pc3.1 Zeo-NLuc-ABCG2 mutants were initially sequenced for the presence of the desired mutation using forward primers SeqF1 for the E211Q mutant, Seq482 for the R482A mutant and both SeqF1 and Seq482 for the double mutant. In mutants validated to express the desired mutation, a full ABCG2 sequencing was carried out covering the whole gene using forward primers Seq482, SeqF2 and SeqF0 and reverse primer SeqR1. All primers were used at a concentration of 100 ng/µL, and sequencing was carried out in-house at the University of Nottingham Deep Sequencing Lab. Upon return of sequence data, chromatograms were analysed using Chromas software version 2.6.6 courtesy of Technelysium pvt Ltd. The full complement of primers used can be seen in **table 2.2**.

Primer	Sequence (5'-3')
Seq482	1337- AACTCTTTGTGGTAGA- 1352
SeqF0	147- GAGTGGCTTTCTACCTTGTC- 166
SeqF1	805-AATGCTTTAAGTGCTTG-826
SeqF2	699- GCAGGGACGAACAATCATCT- 718
SeqR1	339- ATAAATGGAGCACCACGA- 322

Table 2.2. Primers used for full ABCG2 gene sequencing. Primers designed to sequence the entirety of the ABCG2 cDNA when used together. Sequences are given in the 5'-3' direction and numbers indicate the annealing position in the ABCG2 cDNA. Sequences were sequenced in the University of Nottingham Deep Sequencing Lab and analysed using BLAST (NCBI) and Chromas software version 2.6.6.

2.2 ABCG2 expression in mammalian cells

2.2.1 HEK293T cells

HEK239 cells derived by transfection of human embryonic kidney cells with adenovirus 5 were originally generated in 1973 by Alex van der Eb (Graham & van der Eb, 1973). The HEK293T cells (ATCC® CRL-3216™) used in this study are a variant of the HEK293 cell line generated in Michele Calos's lab containing a plasmid encoding the SV40 large T antigen (Lebkowski et al., 1985). This SV40 large T antigen allows for transfections of plasmids carrying the SV40 origin of replication, whilst also maintaining a high copy number.

2.2.2 Cell culture

For routine cell line generation and maintenance, HEK293T cells were cultured in Dulbecco's modified Eagle's medium (DMEM, containing 4.5 g/L D-glucose, 0.11 g/L sodium pyruvate, 0.11 g/L sodium bicarbonate and 0.58 g/L L-glutamine) to which 100 µg/mL penicillin-streptomycin and 10% v/v foetal calf serum (FCS) had been added. The cells were grown until ~70-80% confluency was reached inside T-25

or T-75 flasks incubated in a humidified incubator at 37˚C with 5% CO_2. When the appropriate level of confluency was reached (~3/4 days), cell media was aspirated and cells were carefully washed with PBS. This was then aspirated before cells were detached from the flask by incubation with trypsin for 3 minutes. Following this, complete media was added to deactivate the trypsin and these cell suspensions were spun down at 200 g for 5 minutes. The supernatant was aspirated and cell pellets resuspended in fresh complete media. A sample of cell suspension may then have been taken for cell counting and seeding onto plates/dishes, or otherwise added to a new T25/T75 flask at a 1:10-1:12 dilution with fresh complete media. Finally, where stable cell lines were being maintained, Zeocin (Invitrogen) was added at 40 µg/mL to maintain selection pressure.

2.2.3 Cell counting

10 µL of cell suspension was applied to a Neubauer improved cell counting chamber before being viewed under magnification on a microscope. The average number of cells present in the four 4x4 corner regions were multiplied by 10^4 to calculate the number of cells per mL of each suspension.

2.2.4 PEI transfection

Semi-confluent wild-type HEK293T cells were counted and plated at 250,000 cells in 2 mL media with 10% serum per well of a six-well plate. 24 hours later once the cells had adhered, the media with 10% serum was replaced with media with 5% serum again to a volume of 2 mL per well. A 10 mM linear polyethyleneimine (PEI, Polyscience Inc.) solution was prepared as a transfection reagent of which 9 µL was added to 2 µg of each of the 4 samples of DNA to be transfected (R482A, E211Q, R472A/E211Q and pcDNA-GFP-ABCG2 control). To each DNA/PEI sample, 100 µL of media with 5% serum was added to aid in pipetting dropwise into the corresponding well. Alongside these samples were two control groups: PEI alone (no DNA), and no PEI or DNA. The plate was then briefly tilted to ensure the transfection mixture was evenly distributed within the wells. A stable HEK293T cell line expressing WT pc3.1 Zeo-NLuc-ABCG2 had been previously generated by members of the Kerr Lab, University of Nottingham.

24 hours later the media with 5% serum was replaced with media with 10% serum. A fluorescence microscope was used to examine the GFP-ABCG2 control to give an early indication as to the success of the transfection procedure. After waiting another 24 hours, the well media was removed and the cells detached with trypsin and spun down at 1300 rpm for 5 minutes. The supernatant was removed and the pellet was resuspended in 5 mL media with 10% serum in six T25 flasks. 6 hours later, 10 µL of 100 mg/mL zeocin was added to a final concentration of 200 µg/mL to begin the selection process. The 10% media with serum and zeocin was replaced every 2-3 days, when necessary, until confluency was reached, at which point the cells were transferred to T25 flasks, maintaining the same zeocin concentration. After 10-15 days, when control (no plasmid) transfections showed evidence of complete

cytotoxicity the zeocin concentration was reduced to 40 µg/mL for routine maintenance of the selected cell lines.

2.2.5 Long-term storage of cells

Passages of cells were slowly frozen down to -80˚C to a volume of 1 x 10^6 – 2 x 10^6 cells in 1 mL freezing media per vial, consisting of 90% FCS and 10% DMSO. This initial freezing step was done using a ThermoFisher Mr. Frosty freezing container containing propanol to ensure the optimal rate of cooling of ~1˚C per minute. Cells were then placed into liquid nitrogen for long-term storage at -160˚C. To revive cell lines, frozen suspensions were thawed and incubated in pre-warmed complete media for 24 hours before the media was refreshed to remove DMSO. Complete media was then again refreshed 72 hours later before cell populations were split and restored to media containing zeocin (40 µg/mL) around a week after revival.

2.2.6 Membrane preparation

Cells at 90% confluency were harvested from six 150 mm diameter dishes per cell line and spun down into pellets. These pellets were then resuspended in 10 mL membrane isolation buffer 1 (MIB1) consisting of 10 mM Tris pH 7.4, 250 mM sucrose (8.6%) and 0.2 mM $CaCl_2$, also containing 1:100 dilution of protease inhibitor cocktail III (Calbiochem). This cell suspension was then loaded into a pre-cooled nitrogen cavitation device (Parr Instruments) which was then pressurised to ~750 millibar of nitrogen. The nitrogen cavitation device was left on ice for 20 minutes and carefully shaken halfway through. After this, the cell lysate was slowly collected by releasing the pressure valve, before being placed back into the nitrogen cavitation device and undergoing the process once more. After this, a sample of the lysate was taken and the rest was centrifuged at 1500 g for 15 minutes at 4°C to remove heavy cell debris. A sample of the resulting lysate and pellet resuspended in the same volume of MIB1 were then taken. The lysate was loaded into pre-weighed polyallomer ultracentrifuge tubes and centrifuged at 100,000 g for 45 minutes at 4°C. The supernatant was kept and the pellet weighed to determine the wet mass of cell membranes present. The pellet was then resuspended in a buffer consisting of 20 mM Tris pH 7.4, 250 mM sucrose and 1:100 dilution of protease inhibitor cocktail III. The volume of buffer used was proportional to the calculated wet mass of the membranes at a ratio of 1 mL per 100 mg. The resuspension was then sheared 15 times firstly through a broad 20-gauge needle followed by another 15 times through a narrow 26-gauge needle before being frozen down at -80°C in aliquots of 90 µL each containing ~10 mg of cell membrane.

2.3 ABCG2 protein expression

2.3.1 Bioluminescence imaging

35mm glass-bottomed dishes (Iwaki, 3000-035) were each coated with poly-D-lysine at a concentration of 50 µg/mL for around 90 minutes. Following this, the poly-D-lysine was aspirated and the dishes were washed once in media with 10% serum. Cells of each of the WT and three mutant constructs were counted and plated alongside the GFP-ABCG2 (to act as a control) at 75,000 cells per well in glass-bottomed dishes to a volume of 2 mL. The dishes were then incubated at 37˚C and 5% CO_2 for 48 hours before the cells were ready to be examined at 30x magnification using an Olympus LV200 Bioluminescence Imaging System. Before imaging, the well media was aspirated and replaced with 1.5 mL warm Hank's Buffered Salt Solution (HBSS) and the plates were kept at 37˚C and 5% CO_2. 2 µL furimazine substrate was diluted in 500 µL NanoGlo buffer before being added to the dishes (final concentration of 5 µM) containing HBSS whilst on the microscope to avoid mixing effects of adding the substrate directly. Photos were taken before (bright field) and after (bioluminescence) the furimazine mix was added.

2.3.2 Lowry protein assay

Cell pellets were frozen down before being resuspended in 250 µL ice cold PBS with 10% glycerol and protease inhibitor cocktail III diluted 1:200. Following this, the cell suspension was sonicated (Jencons Scientific LTD- Sonics and materials INC, USA) at 60% power output twice for 10 seconds. Protein concentrations were then determined via a Modified Lowry Protein Assay (BioRad) as per manufacturers protocol. A standard curve was generated using bovine serum albumin (BSA, 0-10 µg protein), and both the standard curve and protein samples were processed in duplicate.

2.3.3 SDS-PAGE electrophoresis

The SDS-PAGE electrophoresis was carried out using Laemmli's method (Laemmli et al., 1977). A consistent quantity of 20-50 µg of each protein sample was made up to a standard well volume of 30-70 µL with PBS and 6X Laemmli buffer containing 2-mercaptoethanol. After this, the samples were incubated at 37˚C for 30 minutes before being loaded into a 1.5 mm 10% w/v polyacrylamide separating gel (40% acrylamide, 10% SDS, 10% APS, 10 µL TEMED, 4.5 mL separating buffer, and 8.5 mL water) beneath a 4% stacking gel (30% acrylamide, 10% SDS, 10% APS, 7.5 µL TEMED, 3 mL stacking buffer and 7 mL water). This gel was electrophoresed at 120 V in protein running buffer (192 mM glycine, 205 mM Tris base and 35 mM SDS) until samples had reached the bottom of the gel (~2 hours). Samples were run in duplicate, and after SDS-PAGE half of the gel was removed for protein visualisation via InstantBlue (Expedeon) Coomassie staining.

2.3.4 Western blotting

The remaining half of the gel underwent wet protein transfer onto nitrocellulose membrane (Amersham) via electroblotting in transfer buffer (192 mM glycine, 25 mM Tris base and 20% v/v methanol) at 200 mA for ~2 hours. The membrane was then stained with Ponceau S to allow for visualisation and marking of the protein lanes and ladder markers. After this, the membrane was washed with PBS-Tween (0.1% v/v) to remove the stain before being blocked in a standard blocking buffer consisting of PBS-Tween supplemented with 5% w/v skimmed milk powder for an hour at room temperature. Once this nonspecific binding was blocked, the membrane was incubated in blocking buffer with PBS-Tween with primary monoclonal mouse antibody (Merck Milipore, BXP-21, 1:2000 dilution in non-fat milk) for ~1 hour at room temperature. Following this, the membrane was washed three times for 5 minutes each in PBS-Tween before being incubated in blocking buffer with secondary antibody (Agilent Dako, rabbit anti-mouse-HRP conjugate, 1:5000 dilution in non-fat milk) for around an hour. Finally the membrane was again washed 3 times for 5 minutes each in PBS-Tween before being incubated for 60 s in enhanced chemiluminescence reagent, ECL (Thermo Scientific, Supersignal West Pico) and subsequently photographed using a Fuji LAS-3000.

2.4 ABCG2 NanoBRET assays

2.4.1 Cell-based NanoBRET binding assays

Cells were seeded in poly-D-lysine treated clear-bottomed white 96 well plates (Greiner, 655-098) at 30,000 cells per well in media with 10% serum. After 24 hours the media was replaced with 37˚C HBSS containing a range of concentrations of mitoxantrone or rhodamine 123 in the absence or presence of ABCG2 inhibitor Ko143. Furimazine solution for all NanoBRET assays was prepared fresh beforehand and consisted of 20 µL substrate per mL NanoGlo buffer (1:50 dilution). 10 µL of this furimazine solution was added to every well (~1 mL per plate) for a final well volume of ~10 µM before the plate was incubated in the dark for 5 minutes. Finally, the bioluminescence and BRET were measured at room temperature using a PHERAstar FS plate reader (BMG Labtech). Filtered light emissions of each well at 685 nm for mitoxantrone and 528 nm for rhodamine 123 were measured and divided by NanoLuc emission at 460 nm to calculate the BRET ratio. Three consecutive repeats of one second per well (~5 minutes in total) were taken for each plate and the data from the second of these was used for analysis. BRET ratios were plotted against a logarithmic scale of drug concentration and data fitted as non-linear regression in GraphPad Prism.

2.4.2 Membrane-based NanoBRET binding assays

Sheared cell membranes were diluted in a 50 mM Tris pH 7.4 buffer supplemented with 0.5% saponin, 0.2% BSA or neither and were plated at 0.5 µg, 2.5 µg or 20 µg membranes per well in clear-bottomed white 96-well plates containing a concentration range of mitoxantrone or rhodamine 123 either with or

without a range of Ko143 concentrations. The bioluminescence and fluorescence values were then measured as at room temperature using the PHERAstar FS plate reader both before and after the addition of furimazine as above. Before this, the non-BRET-specific fluorescence levels were also measured using light excitation via the PHERAstar FS.

2.4.3 Mitoxantrone fluorescence read

To assess whether mitoxantrone had suitable spectral properties for use in BRET assays, an excitation/emission scan was carried out. In this scan, a 96 well plate containing a concentration range of mitoxantrone was excited from 517-574 nm and emission was read at 650 +/- 50 nm. This data was plotted as a scatter graph.

2.4.4 Membrane concentration bioluminescence read

To establish a linear association between membrane concentration and bioluminescence, a concentration range of each membrane suspension was plated on a 96-well plate before 10 µL furimazine was added to each well. Following this, bioluminescence was measured and the mean was fitted as non-linear regression against a logarithmic scale of drug concentration.

3.0 Results

3.1 Mutant plasmid generation, transformation, and purification

Wild type pc3.1 Zeo-NLuc-ABCG2 plasmids were available and ready for use, but the creation of three mutant plasmids with altered substrate interaction would allow for the wider study of NanoBRET as a tool to study ABCG2: substrate interactions. Firstly, the E211Q mutation should lock the transporter in a state with low affinity for substrate (McDevitt et al., 2009). Secondly, the R482A mutation should widen the substrate specificity of ABCG2 (Ejendal et al., 2006). Finally, the R482A/E211Q double mutant should combine these effects.

The three mutant pc3.1 Zeo-NLuc-ABCG2 plasmid constructs were generated using the pre-designed mutagenic primers discussed in section 2.1.1. This vector features a CMV promotor region for high gene expression levels, an ampicillin resistance gene for bacterial selection and a Zeocin resistance gene for cell selection. Incorporated into the vector is the ABCG2 cDNA itself fused to bioluminescent luciferase NLuc via the N-terminus. A schematic of this plasmid is shown previously in **figure 2.1**. Generation of the double mutant used the verified R482A plasmid as the template DNA alongside the E211Q primers to introduce the mutation. PCR was carried out as described in section 2.1.2, before vector template DNA was digested with DpnI and electrophoresed on an agarose gel to confirm total plasmid length, seen in panel A of **figure 3.1.** Bands were present for all 3 PCR products at the expect weight of ~8.1 kb. After this, the plasmids were then transformed into DH5-α competent *E. coli* and purified as per the method discussed in section 2.1.4. Samples of these purified *E. coli* plasmids were digested with restriction

enzyme PvuII to verify the size of the plasmid. These digests were then electrophoresed on an agarose gel for visualisation as displayed in panel B of **figure 3.1**. All three constructs digested into fragments of the expected sizes, confirming that the plasmid was of the intended length of ~8.1kb and the restriction sites were in the correct place. After this, samples of the plasmids were sent for Sanger sequencing.

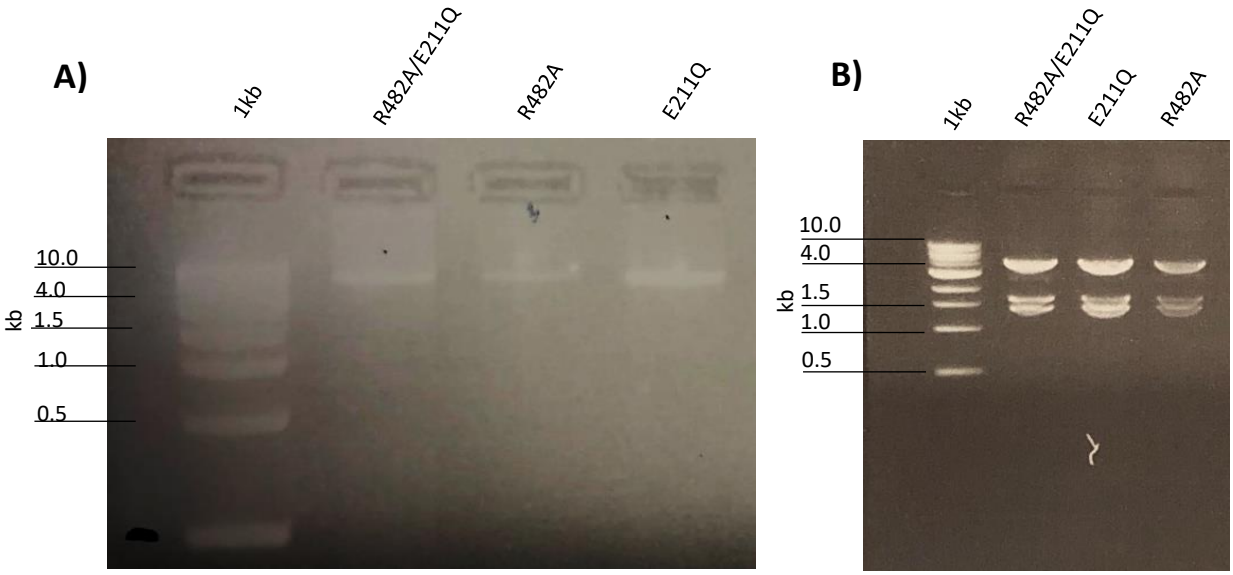

Figure 3.1. Generation of pc3.1 Zeo-NLuc-ABCG2 mutants. A) DpnI digested PCR products. The three PCR products underwent DpnI digestion to remove template DNA. The products of this digest were then electrophoresed under the standard protocol. All 3 constructs show bands between 4 and 10 kb alongside a 1 kb ladder. **B) PvuII digested plasmids.** Purified mutant plasmids were digested with restriction enzyme PvuII and electrophoresed on agarose gel to verify the fragments were of correct length. Fragments shown are of ~ 1.4, 1.7 and 5.0 kb for R482A/E211Q (750 ng/µL), E211Q (533 ng/µL) and R482A (474 ng/µL) alongside a 1kb DNA ladder. The presence of these three bands confirms the identity of the pc 3.1Zeo-NLuc-ABCG2 plasmid which is ~ 8100 bases in length. PCR products were generated with assistance from Deb Briggs.

3.2 Plasmid sequencing

The three mutant plasmids were then sequenced in-house at the University of Nottingham Deep Sequencing Lab to verify the presence of the correct mutation. The sequencing results were analysed using Chromas. The analysis for both R482A and E211Q mutant plasmids can be seen in **figure 3.2** panels A and B using the Seq482 and SeqF1 primers respectively. The mutations of interest (AGG -> GCG for R482A and GAG -> CAA for E211Q) are shown in the red boxes**.** The sequences of all three mutants were examined alongside the WT sequence using BLAST to identify the desired mutation, and all three constructs displayed their respective mutations. Therefore, they were sent for full cDNA sequencing using the full complement of primers discussed in section 2.1.7. The full sequences showed no inadvertent errors and so the plasmids were ready to be transfected into HEK293T cells.

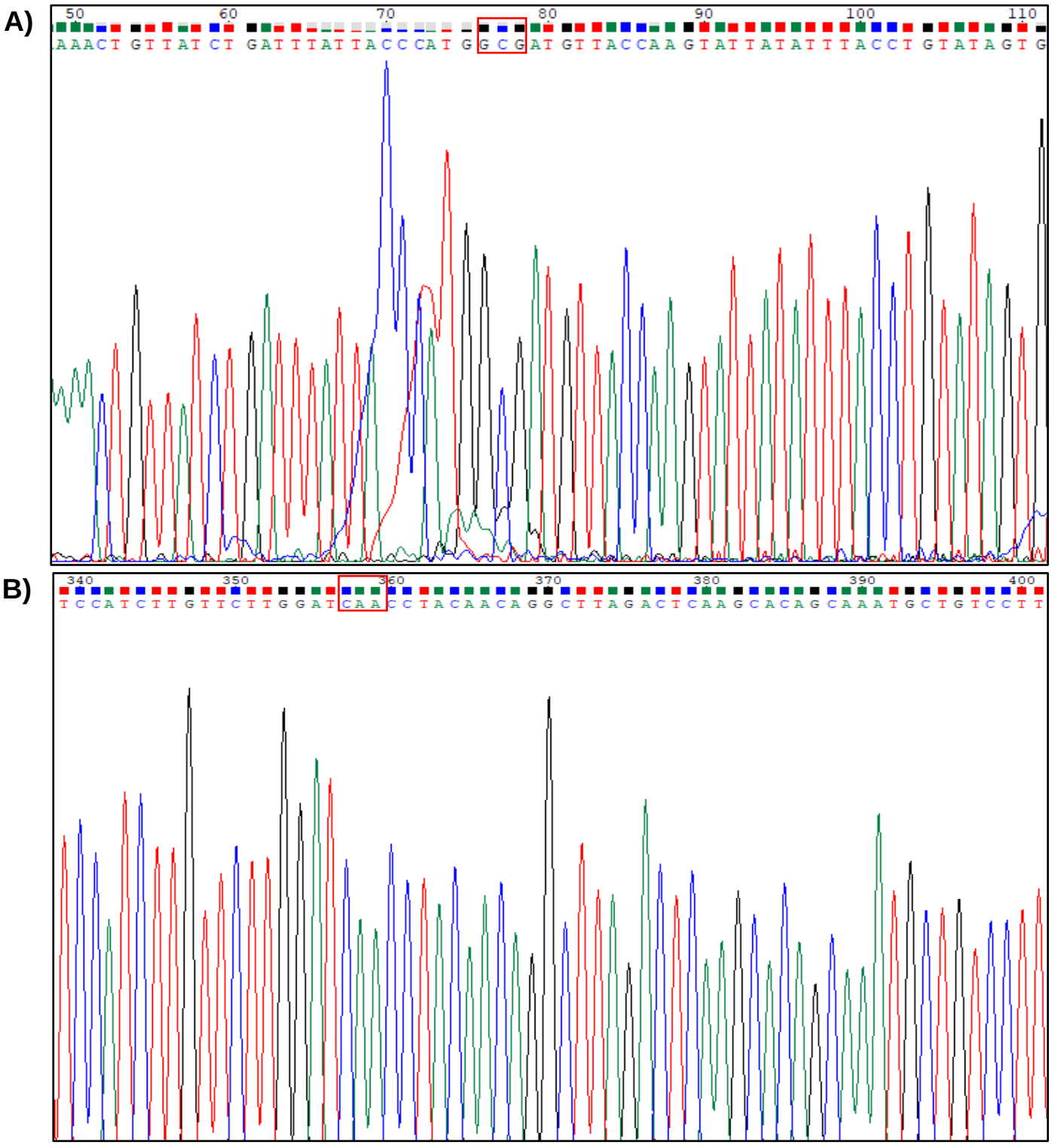

Figure 3.2. Chromatograms of the A) R482A mutation highlighted in the red box at position 76, AGG in WT ABCG2 becomes GCG in R482A. **and B) E211Q** mutation is highlighted in the red box at position 357, GAG in WT ABCG2 becomes CAA in E211Q. Sequencing data was obtained in-house at the University of Nottingham Deep Sequencing Lab using the SeqF0 primer in combination with the E211Q mutant plasmid. Chromatogram was analysed using Chromas software version 2.6.6.

3.3 Plasmid transfection with bioluminescence imaging

The fully sequenced and verified plasmids were then transfected into HEK293T cells as per the method described in section 2.2.4. Alongside this, a plasmid containing GFP was also transfected at the same time to give an early indication of transfection success. These cells expressed fluorescence under a fluorescence microscope and so indicated that the transfection process had been successful. After the transfection and zeocin selection process had finished, cells were plated onto glass-bottom dishes to be examined under a bioluminescence microscope. The improved brightness and image clarity provided by the NanoLuc luciferase in combination with the Olympus LV200 bioluminescence imaging system allowed for high resolution images of transfected HEK293T cells expressing ABCG2 protein. Despite being purely qualitative in nature, the images seen in **figure 3.3** clearly show a successful transfection and selection process of HEK293T cells with pc3.1 Zeo-NLuc-ABCG2 plasmid vector. Panels A and B show the same population of untransfected HEK293T cells under light microscopy and bioluminescence imaging respectively. As expected, the addition of furimazine and filtering for bioluminescence produces no signal in untransfected HEK293T cells. Panels C, D, E and F show populations of transfected cells exhibiting bioluminescence upon addition of furimazine. Aside from confirming the success of transfection and selection, these images also allow us to identify the trafficking of ABCG2 to the cell membrane. The data seen **in figure 3.8** later verifies this by showing high levels of bioluminescence consistent with the expression of NLuc-ABCG2 in the membrane. Therefore, further techniques were not needed to verify that the correct protein trafficking had taken place.

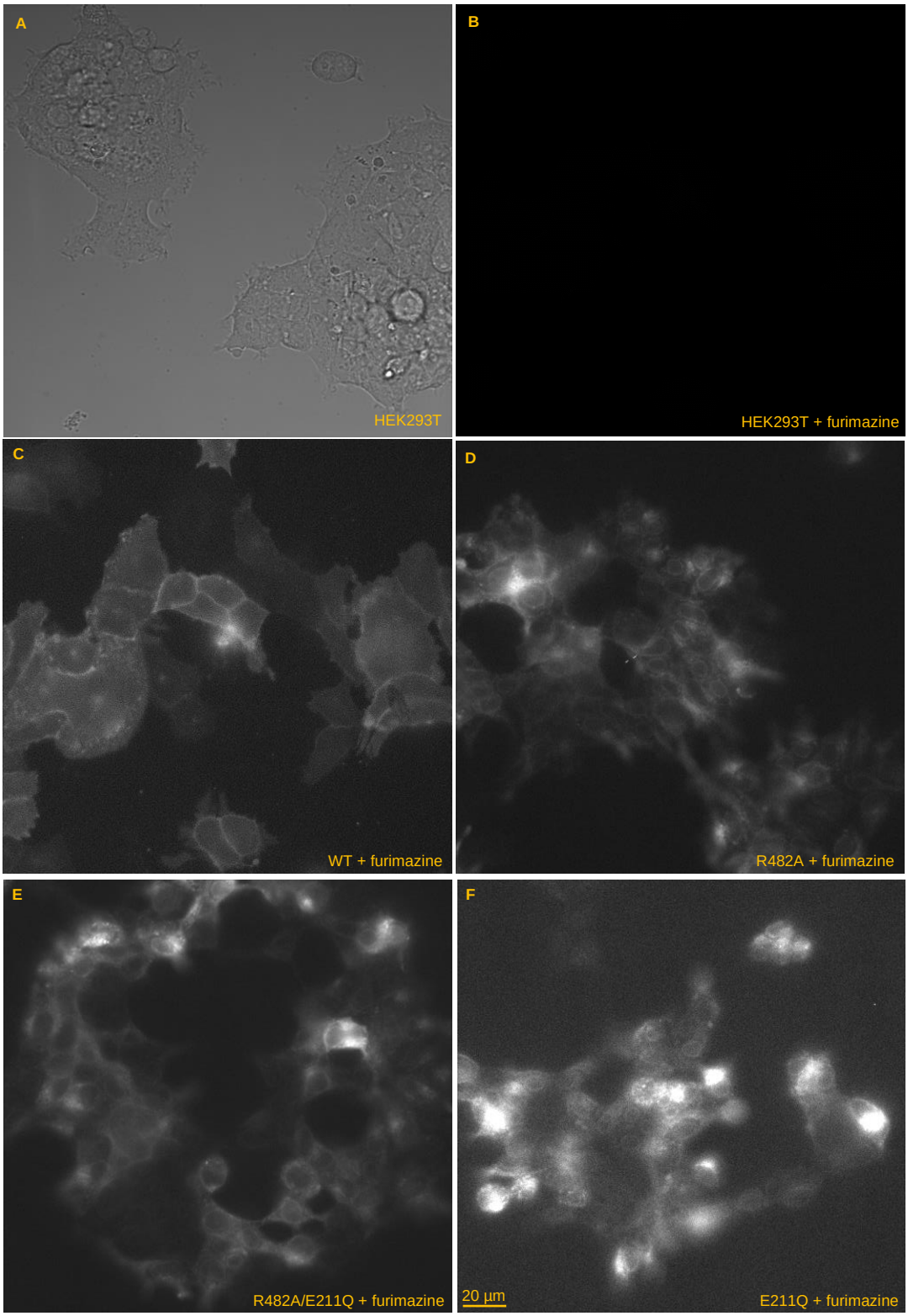

Figure 3.3. Bioluminescence of NLuc-ABCG2 constructs expressed in HEK293T cells. Untransfected HEK293T cells were plated alongside transfected HEK293T cells expressing the four ABCG2 constructs at 75,000 cells per dish in glass-bottom dishes pre-treated with poly-D-lysine. The dishes were then incubated under standard conditions for 48 hours before media was removed and replaced with warm HBSS. The cells were then examined before and after the addition of 10 µL furimazine examined at 30x magnification using an Olympus LV200 Bioluminescence Imaging System. Panels A and B show untransfected HEK293T cells under light microscope and bioluminescence imaging after addition of furimazine respectively. Panels C, D, E and F show HEK293T cells expressing WT, R482A, E211Q and R482A/E211Q ABCG2 constructs respectively under bioluminescence imaging after addition of furimazine.

3.4 Protein assays

Cell pellets expressing ABCG2 constructs were lysed, electrophoresed, and immunoblotted to confirm presence of the ABCG2 protein. Protein was visible on both acrylamide gel and nitrocellulose membrane following Coomassie and Ponceau S staining respectively. In **figure 3.4**, faint bands can be seen for all 3 experimental ABCG2 constructs between 98 and 148 kDa whereas ABCG2 (72.3 kDa) tagged with NanoLuc (17.2 kDa) should be around 90 kDa. However, it is not unexpected for membrane protein bands to be slightly higher than those of the protein standards due to interactions with SDS molecules (Rath et al., 2009). There is also a very faint band in the F439A ABCG2 mutant positive control at around the same kDa. Whilst these figures aren't of great quality, the data seen in **figure 3.3** had already shown NLuc-ABCG2 being expressed and so the project progressed into the experimental stage.

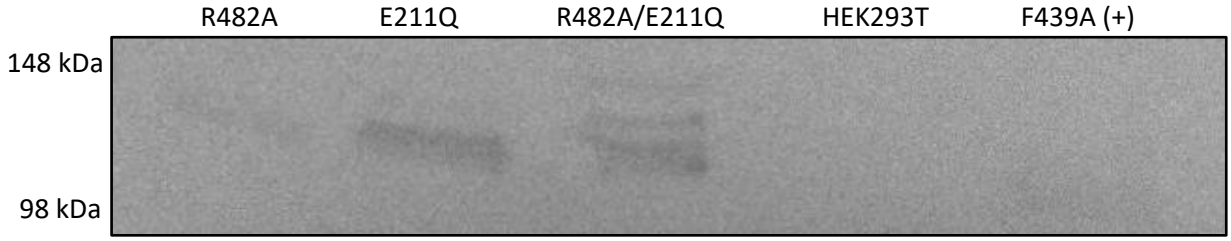

Figure 3.4. Immunoblot of ABCG2 construct lysates. 35 µg of whole cell lysates were electrophoresed in duplicate via SDS-PAGE before being stained and/or Western blotted. Half of the nitrocellulose membrane was transiently stained with Ponceau S to visualise protein bands and mark lanes before being washed with dH_2O and sent on for immunoblotting against primary (BXP-21) and secondary (rabbit anti-mouse HRP conjugate) antibodies. The remaining half of the gel was removed for Coomassie staining with Expedeon Brilliant Blue.

3.5 Cell-based NanoBRET assays with MX

Despite concerns about potential interference caused by cell-based NanoBRET assays due to cellular processes like drug transport or metabolism, the impact of the COVID-19 pandemic on equipment, training and lab restrictions meant that these assays could be carried out immediately. Firstly, a NanoBRET assay was carried out using the WT and E211Q ABCG2-expressing cells at a standard cell density (30,000 cells per well) with a concentration range of MX from 10 nM - 10 µM either with or without a single fixed concentration (1 µM) of the ABCG2 inhibitor Ko143 (**see section 1.11**). This assay was performed to acquire and identify differences between MX dose-response curves for WT and E211Q, as well as to assess whether Ko143 had any effect. As seen in **figure 3.5,** it was clear that a number of the lower concentrations of MX were producing the same baseline level of BRET. Therefore, a follow-up assay was devised using a refined range of MX concentrations from 80 nM - 5 µM, again with the WT and E211Q constructs. This also allowed for the effect of Ko143 to be assessed using multiple concentrations (10 nM - 1 µM), as seen in **figure 3.6**.

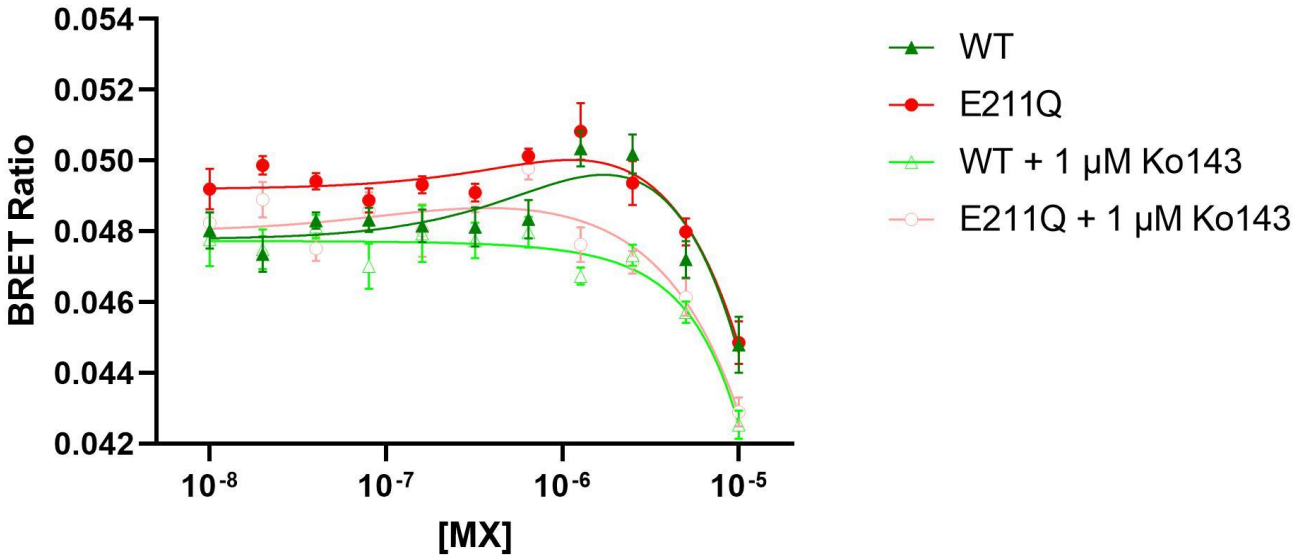

Figure 3.5. BRET observed following MX addition to NLuc-ABCG2 cells. WT and E211Q ABCG2-expressing HEK293T cells were plated in complete media at 30,000 cells per well in a clear-bottom 96-well plate pre-treated with 10 µg/mL poly-D-lysine (Sigma-Aldrich, Missouri USA) and incubated for 24 hours. A concentration range of 30 nM - 10 µM MX either in the absence or presence of 1 µM Ko143 was added, as well as 10 µL furimazine (Promega, Wisconsin, USA) per well. Filtered bioluminescence and fluorescence values for each well were read with a 610+ nm long-pass filter on a BMG LABTECH PHERAstar plate reader after 5 minutes incubation. BRET ratios were calculated by dividing fluorescence emission by bioluminescence emission. Background fluorescence and bioluminescence was removed via subtraction of corresponding 0.5% DMSO BRET ratios. Data plotted is non-linear regression of BRET ratio ± SEM from three technical repeats of one experiment.

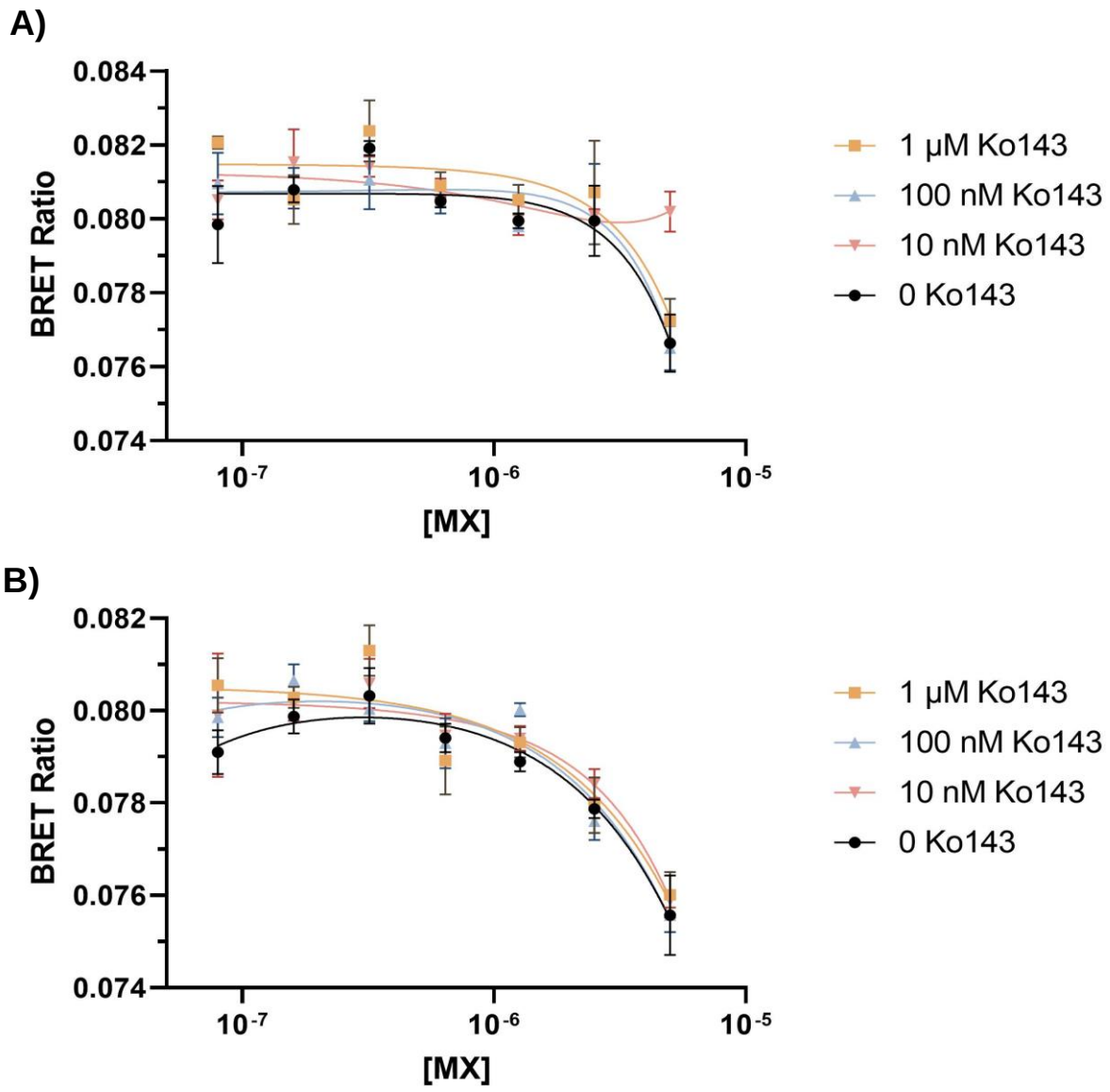

Figure 3.6. BRET observed following MX addition to NLuc-ABCG2 cells with range of inhibitor Ko143. A) WT and **B) E211Q** ABCG2-expressing HEK293T cells were plated in complete media at 30,000 cells per well in a clear-bottom 96-well plate pre-treated with 10 µg/mL poly-D-lysine and incubated for 24 hours. A refined concentration range of 80 nM - 5 µM MX containing 1 µM, 100 nM, 10 nM or no Ko143 was added, as well as 10 µL furimazine per well. Filtered bioluminescence and fluorescence emission values for each well were read with a 610+ nm long-pass filter on a BMG LABTECH PHERAstar plate reader after 5 minutes incubation. BRET ratios were calculated by dividing fluorescence emission by bioluminescence emission. Background fluorescence and bioluminescence was removed via subtraction of corresponding 0.5% DMSO BRET ratios. Data plotted is non-linear regression of BRET ratio ± SEM from three technical repeats of one experiment.

Both WT and E211Q follow the same general trend as seen in **figure 3.5**, with a decrease in BRET ratio as MX concentration increases. This trend goes directly against the hypothesis which stated that BRET ratio should increase with drug concentration. Finally, there was no significant impact of any concentration of Ko143 on BRET ratio. Taken together, these three factors made it clear that some aspect of the experimental design wasn't working as intended. The trends seen in **figures 3.5 and 3.6** were inconsistent and didn't match the hypothesis. However, as previously discussed, it was not

unexpected that the use of whole cells for NanoBRET assays might introduce complications. Therefore membrane suspensions of each construct were prepared for subsequent assays. It is also worth noting that between the two assays there didn't seem to be a significant difference in BRET ratio between the WT and E211Q ABCG2 constructs. However, at this stage it was too early to comment given the assay was still under optimisation.

3.6 Cell membrane NanoBRET assays with MX

Once the membranes were prepared a bioluminescence assay was carried out to verify the process had been successful and that NLuc-ABCG2 was still intact. A concentration range from 12.5 µg - 100 µg of each membrane construct was plated in a 96-well plate before 10 µL furimazine was added to each well and bioluminescence read. As expected, and seen in **figure 3.7**, there was a positive linear correlation between membrane quantity and bioluminescence. There were variations in bioluminescence between constructs with the R482A single mutant exhibiting significantly lower counts than the other mutants, indicative of lower NLuc-ABCG2 expression. Despite this, the data shown in the figure suggested the membrane preparation had been a success and so an assay using membranes with MX was devised. The assay was carried out using the previous concentration range of MX with 2.5 µg of membranes per well. Despite the BRET ratio increasing two-fold when compared to cells, as seen in **figure 3.8**, indicative of an increased transfer of energy, the data still seemed to be inconsistent and continued the general trend of decreasing BRET ratio with increasing MX concentration. This seemed to suggest that the issue with the assay may not have been the system itself (cells/membranes) but instead could have been the specific steric or spectral properties of mitoxantrone as the fluorophore.

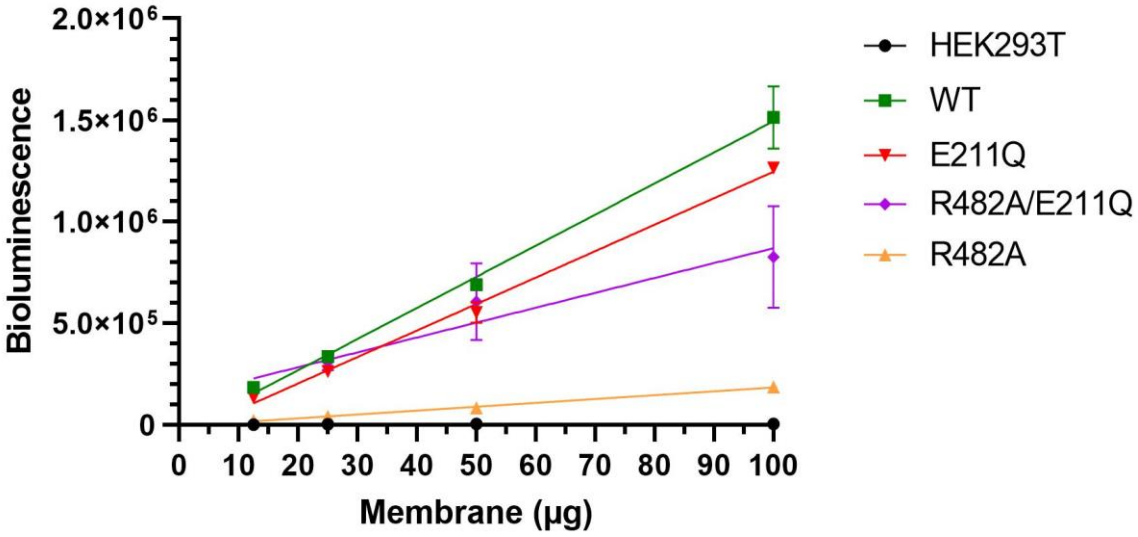

Figure 3.7. Bioluminescence of ABCG2 constructs shows linear dependence on membrane quantity. Four quantities of cell membranes (100, 50, 25 and 12.5 µg) of all four ABCG2 constructs (WT, E211Q, R482A and R482A/E211Q) and untransfected HEK293T cells were plated on a clear-bottom 96 well plate. 10 µL furimazine was added to each well before filtered bioluminescence emission for each well was read using a 460 nm (80 nm bandpass) filter on a BMG LABTECH PHERAstar plate reader after 5 minutes incubation. Data plotted is a linear regression of bioluminescence values ± SEM from three technical repeats of one experiment.

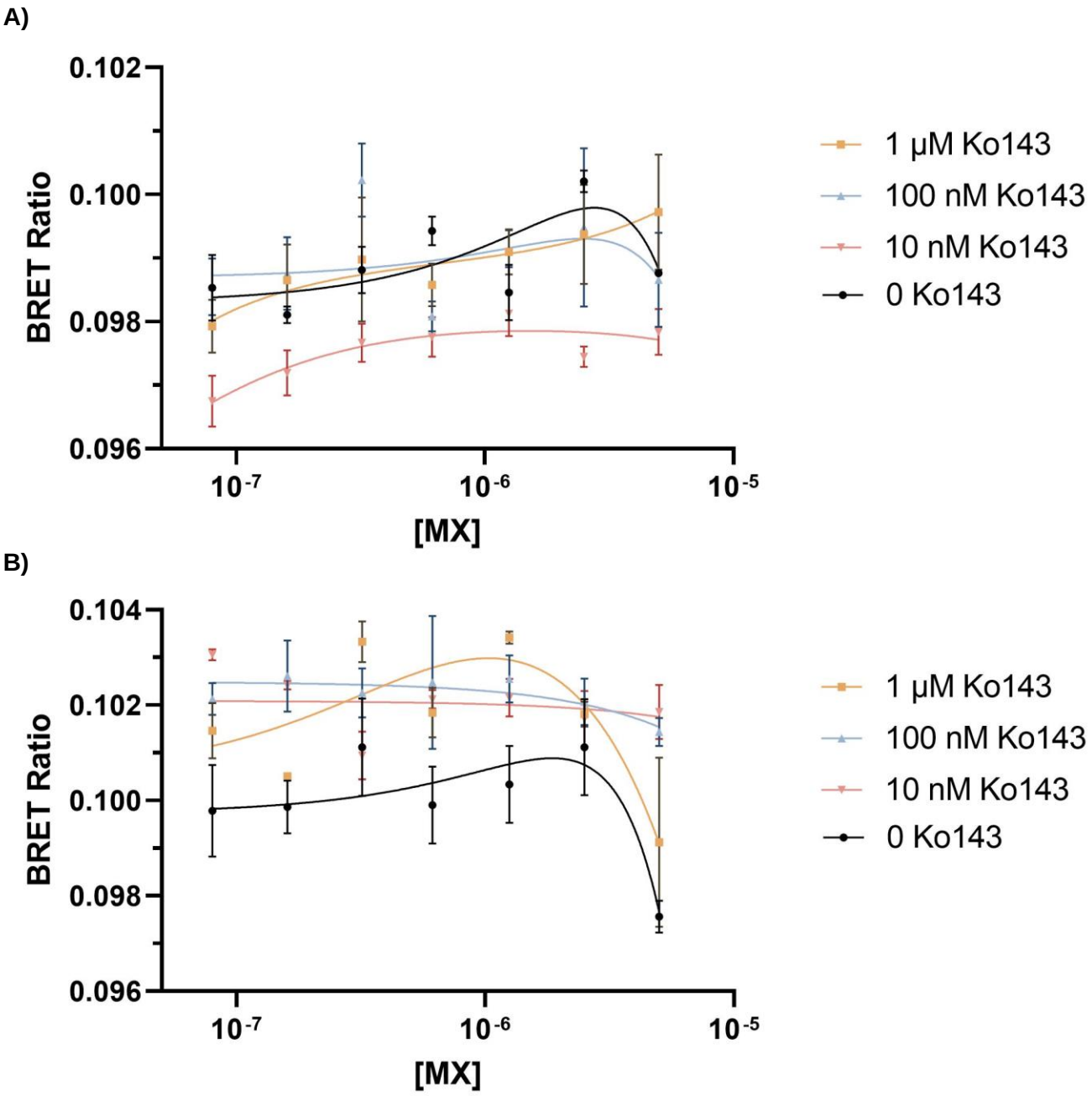

Figure 3.8. BRET with 2.5 µg NLuc-ABCG2 cell membranes and range of inhibitor Ko143. A) WT and **B) E211Q** cell membranes were plated at 2.5 µg membranes per well in a clear-bottom 96-well plate. A refined concentration range of 80 nM – 5 µM MX containing 1 µM, 100 nM, 10 nM or no Ko143 was added, as well as 10 µL furimazine per well. Filtered bioluminescence and fluorescence emission values for each well were read with a >610 nm (longpass) filter on a BMG LABTECH PHERAstar plate reader after 5 minutes incubation. BRET ratios were calculated by dividing fluorescence emission by bioluminescence emission. Background fluorescence and bioluminescence was removed via subtraction of corresponding 0.5% DMSO BRET ratios. Data plotted is non-linear regression of BRET ratio ± SEM from three technical repeats of one experiment.

3.7 The use of mitoxantrone in NanoBRET assays

Mitoxantrone is relatively red-shifted for use as a fluorophore in NanoBRET assays, with a peak excitation of around 610 nm. As discussed previously NanoLuc has a peak emission of around 460 nm, however, there is literature detailing the successful use of fluorophores even further red-shifted than mitoxantrone for NanoBRET assays with just 1-2% spectral crossover (Stoddart et al., 2018). Given that was the case, an excitation/emission assay was carried out on a range of mitoxantrone concentrations to determine its spectral properties first-hand, as seen in **figure 3.9**. Only the highest two tested concentrations of mitoxantrone (10 µM and 5 µM) resulted in significant fluorescence emission which was observed solely at 550+ nm. As seen in the figure via the overlay of the NanoLuc emission spectra, there is very little overlap remaining between NanoLuc and mitoxantrone above 550 nm. Therefore it is likely that there is very little transfer of energy from NanoLuc donor to mitoxantrone acceptor, especially at concentrations below 10 µM which would correlate with the data we saw in **figures 3.5 and 3.6**. Therefore, a decision was made to switch to an alternative substrate with better spectral overlap, rhodamine 123. To conclude the work with mitoxantrone, it is likely that the spectral properties of mitoxantrone and/or its interaction with NanoLuc may not be well suited to NanoBRET assays in this instance.

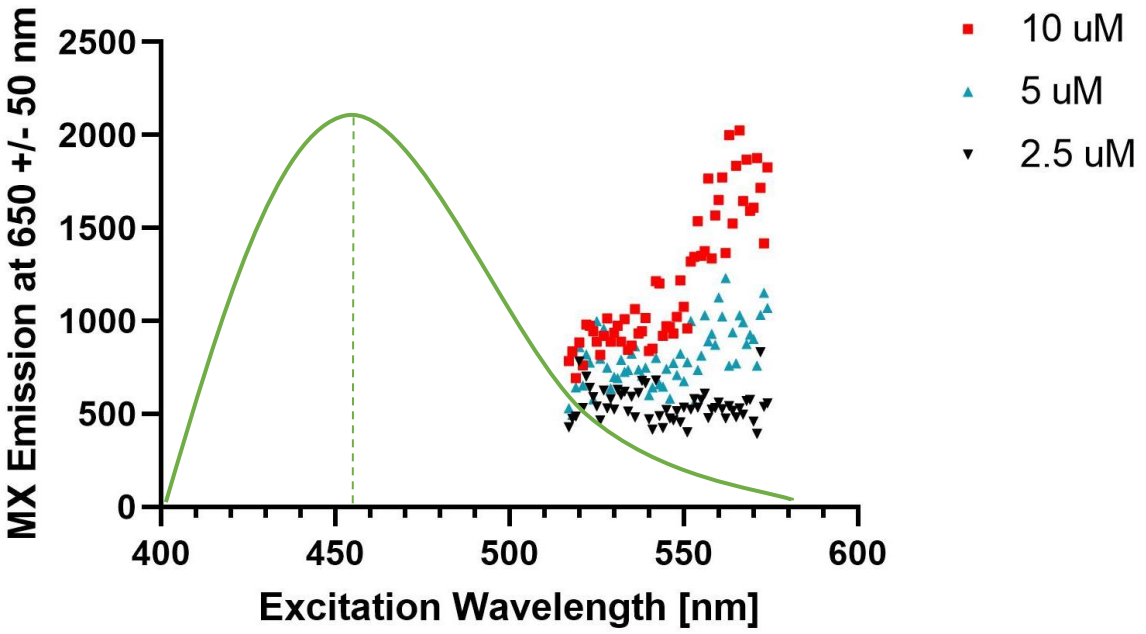

Figure 3.9. The spectral properties of MX may preclude BRET measurements with this ABCG2 substrate. An excitation/emission assay using external fluorescence excitation with a concentration range of 10 nM – 10 µM MX was carried out to determine the spectral properties of MX. MX was excited in a scan from 517-574 nm and emission read at 650 ± 50 nm. Overlaid is the emission curve (green) for the NanoLuc luciferase showing very little spectral crossover between the two species. Also shown is the very high concentration of MX required to receive significant emission. Data shown is raw values from three technical repeats of one experiment.

3.8 Is rhodamine 123 a feasible substrate for ABCG2 NanoBRET?

Changing the fluorescent ligand to rhodamine 123 also meant changing the experimental ABCG2 construct to the R482A/E211Q double mutant, as both the wild type and single E211Q mutant would be incapable of binding R123 (Alqawi et al., 2004). As well as this, **figure 3.7** showed the R482A single mutant to have substantially less bioluminescence than both WT and R482A/E211Q so using the double mutant would allow for a similar volume and concentration of membranes to WT to be used. Consequently, an assay using the standard concentration range of R123 of 10 nM – 10 µM with 2.5 µg membranes per well of both the WT and R482A/E211Q constructs either with or without 10 µM Ko143 was carried out. As seen in **figure 3.10**, the BRET ratio was much higher than the previous assays with MX indicating a greater transfer of energy from G2 to substrate. Critically, this assay using R123 followed the hypothesised trend of increasing BRET ratio with increasing drug concentration. Despite this, the addition of Ko143 appeared to have no effect, with the data points for the Ko143 groups being directly overlaid with their respective groups in the absence of Ko143.

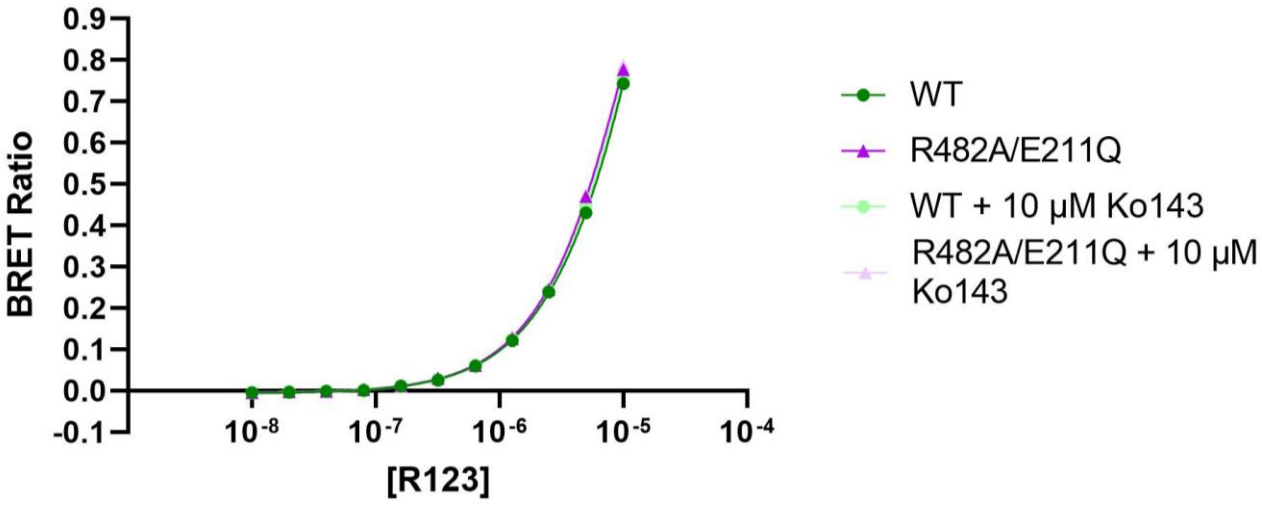

Figure 3.10. BRET with more suitable substrate R123 applied to NLuc-ABCG2 membranes. Cell membranes were plated at 2.5 µg per well in a clear-bottom 96-well plate. The standard concentration range of 10 nM – 10 µM R123 containing 10 µM Ko143 or not was added, as well as 10 µL furimazine per well. Filtered bioluminescence and fluorescence emission values for each well were read with a 460 nm (80 nm bandpass) filter on a BMG LABTECH PHERAstar plate reader after 5 minutes incubation. BRET ratios were calculated by dividing fluorescence emission by bioluminescence emission. Background fluorescence and bioluminescence was removed via subtraction of corresponding 0.5% DMSO BRET ratios. Data plotted is non-linear regression of BRET ratio ± SEM from three technical repeats of one experiment.

However, whilst **figure 3.10** was encouraging in showing a clear dose response, the transporter did not seem to saturate as no plateau was reached at the higher concentrations of R123. ABCG2 should fully saturate as there are a finite number of substrate binding sites available at any one time. This lack of plateau could either be because the affinity of the substrate is just too low to achieve full saturation, or because of an R123 accumulation within the membrane leading to a non-specific ‘bystander BRET’

effect. Practically speaking, bystander BRET suggests a transfer of energy between transporter and unbound substrate within the vicinity of NLuc and would likely mask any specific BRET interactions seen between ABCG2 and substrate. Given that this could be the case, several assays were designed to identify and minimise the effects of this potential bystander BRET.

Three further assays were carried out incorporating changes designed to reduce nonspecific effects, as seen in **Figure 3.11.** The first of these assays shown in **figure 3.11A** included the addition of 0.5% saponin as a detergent to disrupt the ABCG2 membrane vesicles with an increased concentration range of 80 nM - 80 µM R123. The addition of saponin would have prevented an imbalance of inward and outward-facing membrane vesicles and ensured that all ABCG2 binding sites were available in both vesicle orientations. The second assay shown in **figure 3.11B** instead used 0.5 µg cell membranes per well with this increased concentration range of 80 nM - 80 µM R123. Reducing the quantity of membrane would reduce the potential for saturation of the membrane by R123, thereby decreasing the impact of non-specific BRET. The final assay seen in **figure 3.11C** increased membrane quantity to 20 µg membranes per well with the standard concentration range of R123 of 10 nM – 10 µM either with or without 10 µM Ko143. Increasing the volume of membrane would increase the number of ABCG2 binding sites and ensure high availability of the transporter for R123. Unfortunately, the three alterations made in **figure 3.11** did not result in the formation of a plateau phase which indicated that non-specific BRET interactions were still taking place.

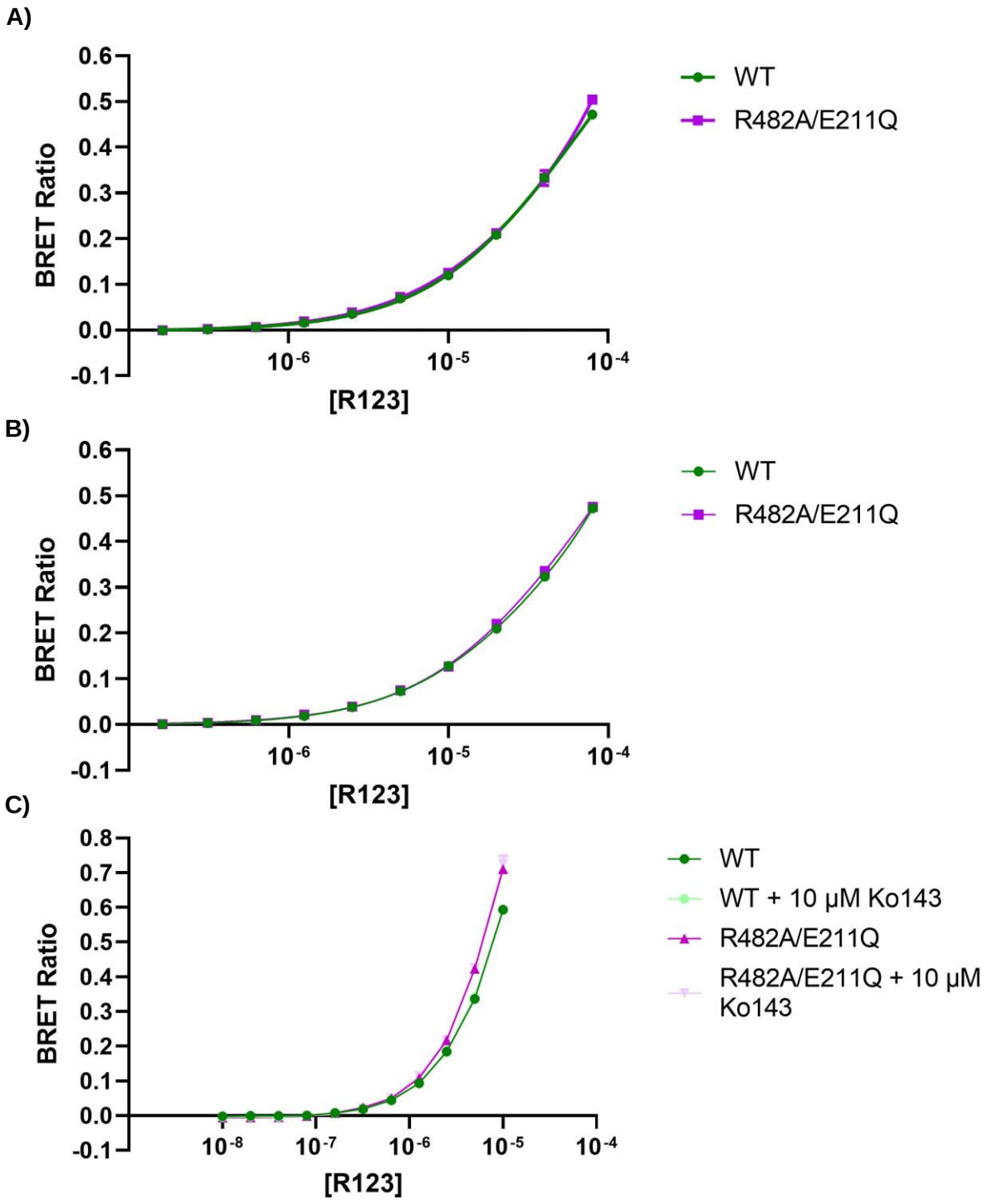

Figure 3.11. Attempts to optimise BRET between NLuc-ABCG2 and R123. Cell membranes were plated in a clear-bottom 96-well plates at **A)** 2.5 µg with an increased concentration range of 80 nM – 80 µM R123 containing 0.5% saponin. **B)** 0.5 µg with an increased concentration range of 80 nM – 80 µM R123. **C)** 20 µg with a standard concentration range of 10 nM – 10 µM R123 containing 10 µM Ko143 or not, all with 10 µL furimazine per well. Filtered bioluminescence and fluorescence emission values for each well were read with a 460 nm (80 nm bandpass) filter on a BMG LABTECH PHERAstar plate reader after 5 minutes incubation in the dark. BRET ratios were calculated by dividing fluorescence emission by bioluminescence emission. Background fluorescence and bioluminescence was removed via subtraction of corresponding 0.5% DMSO BRET ratios. Data plotted is non-linear regression of BRET ratio ± SEM from three technical repeats of one experiment.

3.9 The bystander effect and BRET with cells

To try and identify the extent of the bystander effect an assay was devised incorporating NLuc-tagged beta-2 adrenergic receptor (β_2AR) membranes obtained from Dr Laura Kilpatrick and Dr Mark Soave (COMPARE Lab, University of Nottingham). Any BRET exhibited between the NLuc-tagged β_2AR and R123 would be non-specific as R123 is not characterised as a ligand for β_2AR. An assay of this in parallel with 2.5 µg of ABCG2 membrane constructs with the increased concentration range of R123 of 80 nM – 80 µM was carried out. BSA (0.2%) was also added to the suspensions to reduce the potential of membranes adsorbing to each other or plasticware. The results, as seen in **figure 3.12**, show a nearly identical BRET ratio for β_2AR as with our ABCG2 constructs. However, it is important to note that the β_2AR membranes were prepared under a different protocol as the ABCG2 membranes, and that the NLuc is extracellular in GPCR constructs rather than intracellular in ABCG2. Additionally, the bioluminescence of these control membranes showed considerable variability between experiments. Despite this, the data still seems to indicate a significant proportion of the BRET seen in the ABCG2 membranes may be nonspecific bystander BRET.

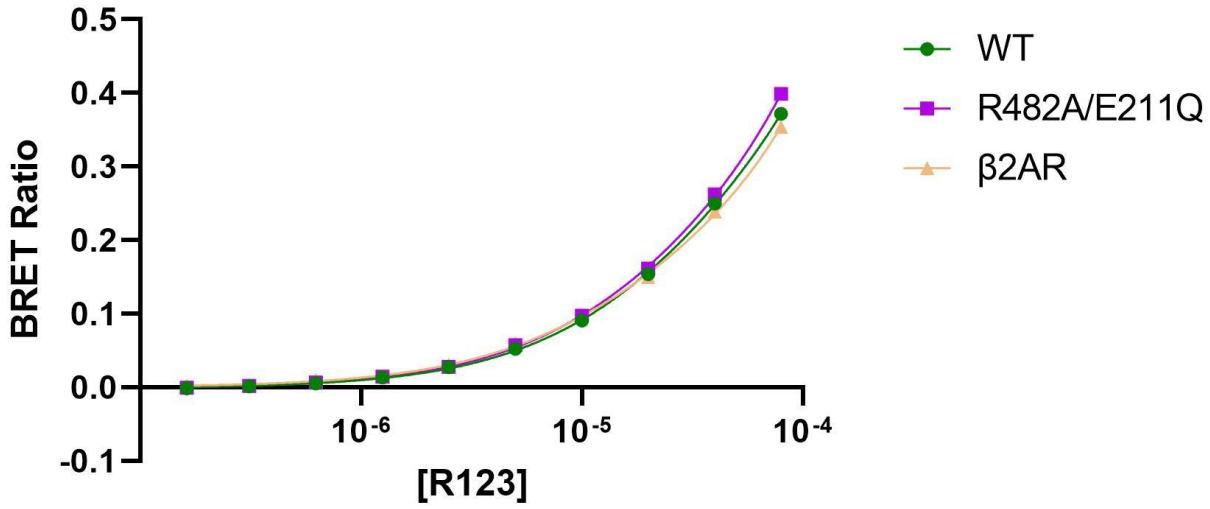

Figure 3.12. Bystander BRET effect appears to be significant. Cell membranes were plated at 2.5 µg membranes per well in a clear-bottom 96-well plate. An increased concentration range of 80 nM – 80 µM R123 containing 0.2% BSA was added, as well as 10 µL furimazine per well. Filtered bioluminescence and fluorescence emission values for each well were read with a 460 nm (80 nm bandpass) filter on a BMG LABTECH PHERAstar plate reader after 5 minutes incubation. BRET ratios were calculated by dividing fluorescence emission by bioluminescence emission. Background fluorescence and bioluminescence was removed via subtraction of corresponding 0.5% DMSO BRET ratios. Data plotted is non-linear regression of BRET ratio ± SEM from one representative of five independent experiments each with three technical repeats.

One final experiment was devised using R123 with whole cells expressing our ABCG2 constructs. The parameters were the same as the previous MX assays with cells, but instead using R123 at the increased concentration range of 80 nM – 80 µM. **Figure 3.13** shows the BRET ratio for the two constructs, again showing the same shape curve as the membrane assays, with no saturation of the ABCG2 transporter by

R123. Therefore the use of rhodamine 123 in NanoBRET assays with the ABCG2 transporter has been unable to produce a BRET signal with specificity to the transporter in this instance

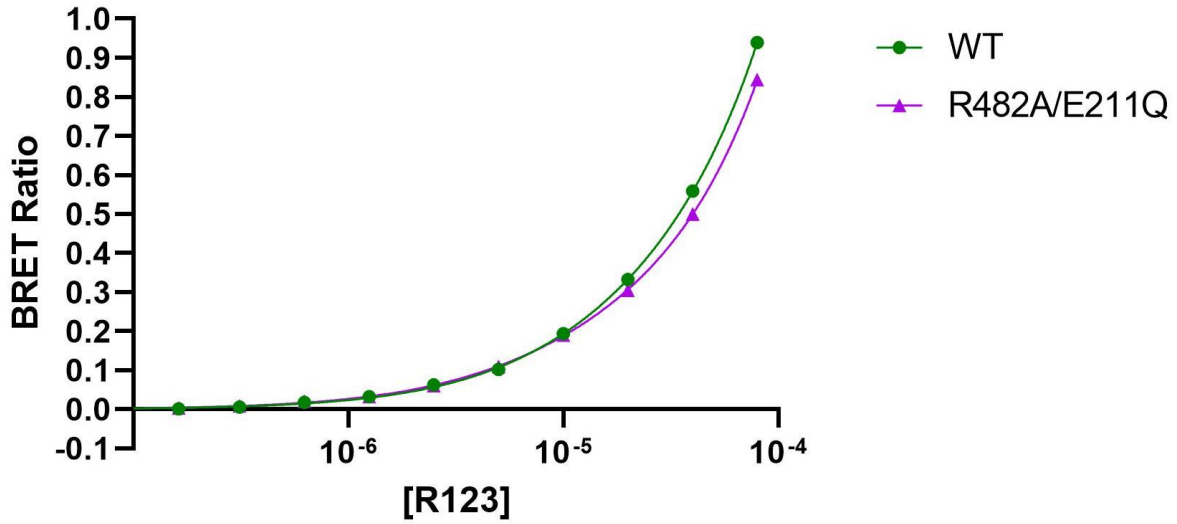

Figure 3.13. NanoBRET can report on ABCG2 and R123 in cells. ABCG2-expressing HEK293T cells were plated in complete media at 30,000 cells per well in a clear-bottom 96-well plate pre-treated with 10 µg/mL poly-D-lysine and incubated for 24 hours. An increased concentration range of 80 nM - 80 µM R123 was added, as well as 10 µL furimazine per well. Filtered bioluminescence and fluorescence emission values for each well were read with a 610+ nm long-pass filter on a BMG LABTECH PHERAstar plate reader after 5 minutes incubation. BRET ratios were calculated by dividing fluorescence emission by bioluminescence emission. Background fluorescence and bioluminescence was removed via subtraction of corresponding 0.5% DMSO BRET ratios. Data plotted is non-linear regression of BRET ratio ± SEM from three technical repeats of one experiment.

4.0 Discussion

4.1 BRET, NLuc and ABCG2

BRET and FRET have been used previously to investigate the oligomerisation of WT ABC transporters expressed in HEK293 cells (Frixel et al., 2016; Ni, Mark, et al., 2010). Despite this, to my knowledge at the time of writing, the present study is the first to use BRET in combination with the ABCG2 transporter and the first to use BRET to examine ABC substrate transport in general. Therefore, there is no BRET ratio data from similar studies with which to compare these findings. Previous assessment of ABCG2 substrate binding and transport activity has been carried out using high-throughput efflux assays coupled with mass spectrometry for quantification (Xiao et al., 2006). These studies are a direct quantification of substrate transport and provide efflux ratios of tested compounds for drug discovery. However, NanoBRET effectively quantifies distance between transporter and substrate instead of directly measuring binding and transport, so comparisons of data further than correlation between these two methods are difficult to draw. This leaves room for a NanoBRET assay to act as an initial screening tool to help identify and narrow down potential ABCG2 substrates and inhibitors before more robust analysis.

In addition, whilst it is theoretically possible that the addition of the NanoLuc tag to ABCG2 could have negatively impacted transport function, the likelihood of this being the case is slim. The NanoBRET system is very well characterised (both commercially by Promega and otherwise in literature) and NLuc itself is also a very small luciferase at ~ 17 kDa which reduces the potential for steric interference with the transporter. The larger FLuc has been used successfully in bioluminescent imaging with its substrate D-luciferin, which also happens to be bindable by ABCG2 (Zhang et al., 2007). Taken together, these factors suggest it to be unlikely that NLuc would have a significant effect on ABCG2 binding activity, but this is something that could and should be confirmed in future ABCG2 NanoBRET studies.

4.2 Summary of results

ABCG2-mediated MDR and related resistance to chemotherapeutics prevents effective cancer treatment. Whilst structures and mechanisms of the ABCG2 transporter are slowly becoming clearer, there is still much to uncover about binding activity and substrate interaction. In principle, BRET could be used to report on these ABCG2: substrate interactions in both WT and mutant transporters, potentially allowing for the screening and optimisation of prospective anti-cancer drugs. To accomplish this, the present study performed NanoBRET assays using NLuc-ABCG2-expressing HEK293T cells and membranes with substrates MX and R123. Through these assays, we demonstrated the ability for BRET to successfully report on ABCG2: R123 binding with a positive dose-response, albeit with some concerns for the long-term use of the assay which will be considered later in the discussion.

The initial assays with mitoxantrone and cells did not follow the hypothesised trend of positive dose-response. Instead, they showed a negative correlation between substrate concentration and BRET ratio, no reliable difference between ABCG2 constructs, and no significant effect of ABCG2 inhibitor Ko143. Despite this, these assays proved helpful in developing and optimising the experimental protocol. After producing the cell membranes, the expected linear relationship between membrane concentration and bioluminescence was demonstrated which indicated a successful membrane preparation in which the NLuc-ABCG2 transporters were intact. This also provided a quantitative measure of the ABCG2 expression levels in each of the constructs. Examining the spectral properties of MX first-hand highlighted its lack of spectral crossover with NLuc, whereas R123 proved to have a more preferable profile for use in ABCG2 NanoBRET assays.

The assays performed subsequently using R123 showed the potential of BRET to be able to report on ABCG2: substrate interactions. Critically, the positive dose-response between increasing substrate concentration and BRET ratio when using R123 in membranes indicates that the fundamental principles of BRET are effective in the context of ABCG2. The BRET ratio values remained relatively consistent between experiments with R123 and membranes which demonstrates high reliability in ACBG2 NanoBRET assays. This gives great confidence in assessing whether NanoBRET is suitable for ABCG2

studies as clearly the NLuc and substrate are within the 10 nm requirement for BRET to take place efficiently.

4.3 Testing of hypotheses

Some of the hypotheses for this project have been proven whilst other aspects have been encouraging but still require further investigation. Firstly, the application of BRET to transporter-substrate interactions with ABCG2 has been a successful proof of concept. Data showing dose-response BRET ratios increasing with substrate concentration has been attained, and it is likely full saturation of the transporter can be achieved with minor refinements to the experimental design (see section 4.4). Furthermore, **figure 3.13** indicates that BRET can be just as effective in producing a dose-response for ABCG2: substrate interactions in cells as well as in membranes. Taken together, these factors show that BRET can be an important tool in future studies of the ABCG2 transporter and its substrates.

Despite this, the range of assays carried out have failed to produce different BRET ratios between any of the tested ABCG2 constructs as hypothesised at the start of the project. It is surprising that this was the case given that there should be differences in substrate binding and transport activity between the mutants in both whole cell and membrane-only environments. That said, it is not unreasonable to theorise that any nonspecific bystander BRET between substrate and ABCG2 transporter could mask the presence of specific interaction, and therefore obscure any differences in BRET ratio between constructs.

This bystander effect may have also played a role in suppressing the hypothesised effect of potent ABCG2 inhibitor Ko143. Given that previous studies have shown Ko143 to be very effective in preventing substrate transport by ABCG2 through competitive binding, it's hard to see how the use of Ko143 wouldn't have an effect on specific BRET interaction (Weidner et al., 2015). Therefore, it may be the case that bystander BRET is occurring to such a degree that the displacement of specific signal by Ko143 cannot yet be measured. Although the apparent extensive impact of the bystander BRET effect has damaged the full testing of our hypothesis, the research carried out in this project has provided an encouraging start to the use of BRET in examining ABCG2 transporter-substrate interactions and has opened various avenues for further research.

4.4 Alternative ideas

The potential nonspecific effects between ABCG2 and fluorescent substrate have undoubtedly been an issue throughout the study. Bystander BRET is a phenomenon well described in existing literature and has been used in numerous studies as a method by which to assess receptor trafficking (Balla et al., 2012). Fluorescently labelled proteins can undergo BRET if located in the same subcellular compartment thereby reporting on trafficking pathways (Namkung et al., 2016). NanoBRET assays similar to those performed in the present study have taken place in GPCRs like β_2AR. These studies quantify nonspecific saturation binding competitively using a non-fluorescent higher-affinity ligand (propranolol) to displace

BRET signal (Stoddart et al., 2015). This allows for a quantitative measure of the bystander effect that may be taking place. Fortunately, the ligands used in such studies often have very high affinity and specificity which means the nonspecific effects are often minimal. If this is not the case, ligands are frequently designed and modified with different linkers and fluorophores to improve and optimise specificity and affinity (Goulding et al., 2021). Consequently, the two natural substrates tested in the present study, MX and R123 are unlikely to have such high specificity and certainly don't have as high an affinity (micromolar range) as ligands used in GPCR (nanomolar range) studies (Ni, Bikadi, et al., 2010). This casts slight doubt over the suitability of ABCG2: substrate interactions for study using NanoBRET as nonspecific effects can be difficult to remove.

Ko143 labelled with Cy5 was tested for BRET with ABCG2-expressing membranes during this study but there was no transfer of energy from NLuc to inhibitor. Initially, this would support an argument of ABCG2: substrate interactions being unsuitable for examination by NanoBRET assays it would seem the fluorescent Ko143 was not in close enough proximity with the NLuc tag for energy transfer to take place. However, the Cy5 tag is very red-shifted with a peak excitation of 650 nm, giving it even less of a spectral overlap than MX. Given the lack of energy transfer seen with MX it is not surprising that no BRET was seen with Cy5-Ko143. Therefore, it is not possible to say whether the affinity of ABCG2 substrates/inhibitors is too low to fully saturate the transporter as the results of this are inconclusive. Further suggestions of how to tackle this issue, including the use of BODIPY-Ko143, are discussed in the next section.

4.5 Future work

As discussed previously, the research carried out on this project has introduced considerable scope for further study into BRET with ACBG2 transporters. One of the main concerns throughout the project was the possibility that the tested substrates had just too low of an affinity to fully saturate the transporter. The aforementioned NanoBRET assay involving higher affinity Cy5-Ko143 was designed to see full saturation of the transporter reflected in a sigmoidal BRET ratio curve. Unfortunately, no BRET was exhibited between ABCG2 and Ko143-Cy5 which wasn't unexpected due to the red-shift of the Cy5 label. Alongside this, the Cy5 tag itself had been suspected of impacting the steric properties of Ko143 in other studies in the Kerr lab, rendering it unreliable as an inhibitor. Therefore one of the key suggestions for further study would be to perform similar assays to the present study with a fluorescently-labelled high affinity substrate or inhibitor with an appropriate spectral profile for sufficient overlap with NLuc. One recommendation for this is BODIPY-labelled Ko143 which has a peak excitation of 503 nm and doesn't appear to have steric clashes with ABCG2. Hopefully, this high-affinity inhibitor would first demonstrate whether Ko143 indeed binds to cavity one akin to substrates by the appearance of a BRET signal, then if so, saturate the transporter and provide a sigmoidal dose-response. Critically, Ko143 is a potent inhibitor in the nanomolar range so this single experiment should allow for the testing of the low-affinity

hypothesis. Unfortunately, BODIPY-Ko143 is not yet available in the lab in the quantities required for full analysis of its interaction with ABCG2.

Also, the differences in preparation and bioluminescence between the NLuc-ABCG2 and NLuc-β_2AR membranes meant that it was not possible to completely verify the extent to which bystander BRET was taking place. As discussed previously, an important side-note to this is to consider whether the specific location of the NanoLuc tag within the protein would have an effect on the interaction with substrate. For both ABCG2 and β_2AR NLuc is located on the N-terminus, however this is inside the cell membrane for ABCG2 and outside the cell membrane for β_2AR. Ideally then, a transporter with the same orientation within the membrane as ABCG2 should be used as the control to remove this variable. To address these concerns, similarly NLuc-tagged cells and membranes exhibiting a different membrane transporter (i.e. not ABCG2) should be grown and harvested as a control by the same person in parallel to the ABCG2 construct-expressing cells and membranes. This would enable a direct comparison of the BRET ratios between specific ABCG2-substrate interactions and non-specific BRET between the same drug and a transporter for which it is not a substrate. This robust control would be free of any differences in NLuc localisation and preparation protocol. Only then would you be able to estimate, with confidence, the degree of bystander BRET taking place in ABCG2 NanoBRET assays. Furthermore, the hydrophobicity of R123 in comparison to propranolol was considered as a possible contributor to nonspecific effects if R123 exhibited increased β_2AR membrane accumulation. Both propranolol and rhodamine 123 are relatively hydrophobic with solubilities in ethanol of 30 mg/mL and 20 mg/mL respectively (Laurens et al., 2019; Bhattarai et al., 2020). Therefore it is unlikely that excess nonspecific effects were caused by increased R123 accumulation in β_2AR membranes compared to propranolol.

Finally, an interesting follow-up to the present study could be the examination of BRET with ABCG2 transporters purified with styrene maleic acid (SMA) co-polymers. This detergent-less method produces lipid particles consisting of solubilised discs of membrane bilayer surrounded by SMA known as SMA lipid particles (SMALPs, Gulati et al., 2014). This means transporters can be purified in their natural lipid environment without disruption by detergents, thereby exhibiting increased stability and purity compared to detergent-based solubilisation methods. Any specific BRET interactions seen between substrate and ABCG2 may benefit from this more representative transporter environment, and so ACBG2 SMALPs may prove to be an effective system for further NanoBRET studies.

4.6 Conclusion

The assays performed throughout this project are the first of their kind in using BRET to report on ABCG2: substrate activity. The data received has provided a good starting point for further research into how BRET can be best used in this field, and it is clear that there is scope for BRET to report on the binding activity of ABCG2 and its substrates at the very least. If the nonspecific interactions seen with nanoBRET studies in ABCG2 can be identified and minimised, further substrates and inhibitors can be

examined. Therefore, the future application of BRET to ABCG2 could reveal structural and binding information about the transporter leading to the structural optimisation of anti-cancer drugs and screening of new ABCG2 inhibitors. As discussed in section 1.16, the development of an effective BRET assay for ABCG2 would not only assist our understanding of its structure and mechanisms but could also aid in drug discovery given that all new drugs are tested for ABCG2 interactions. Hopefully, this in turn can result in more effective chemotherapy and improved cancer prognoses.

5.0 References

Abbott, B. L., Colapietro, A.-M., Barnes, Y., Marini, F., Andreeff, M., & Sorrentino, B. P. (2002). Low levels of ABCG2 expression in adult AML blast samples. *Blood*, *100*(13), 4594–4601. https://doi.org/10.1182/blood-2002-01-0271

Allen, J. D., van Loevezijn, A., Lakhai, J. M., van der Valk, M., van Tellingen, O., Reid, G., Schellens, J. H. M., Koomen, G.-J., & Schinkel, A. H. (2002). Potent and specific inhibition of the breast cancer resistance protein multidrug transporter in vitro and in mouse intestine by a novel analogue of fumitremorgin C. *Molecular Cancer Therapeutics*, *1*(6), 417–425.

Allikmets, R., Schriml, L. M., Hutchinson, A., Romano-Spica, V., & Dean, M. (1998). A human placenta-specific ATP-binding cassette gene (ABCP) on chromosome 4q22 that is involved in multidrug resistance. *Cancer Research*, *58*(23), 5337–5339.

Alqawi, O., Bates, S., & Georges, E. (2004). Arginine482 to threonine mutation in the breast cancer resistance protein ABCG2 inhibits rhodamine 123 transport while increasing binding. *The Biochemical Journal*, *382*(Pt 2), 711–716. https://doi.org/10.1042/BJ20040355

Balla, A., Tóth, D. J., Soltész-Katona, E., Szakadáti, G., Erdélyi, L. S., Várnai, P., & Hunyady, L. (2012). Mapping of the Localization of Type 1 Angiotensin Receptor in Membrane Microdomains Using Bioluminescence Resonance Energy Transfer-based Sensors *. *Journal of Biological Chemistry*, *287*(12), 9090–9099. https://doi.org/10.1074/jbc.M111.293944

Bhattarai, N., Chen, M., L. Pérez, R., Ravula, S., M. Strongin, R., McDonough, K., & M. Warner, I. (2020). Comparison of Chemotherapeutic Activities of Rhodamine-Based GUMBOS and NanoGUMBOS. *Molecules*, *25*(14). https://doi.org/10.3390/molecules25143272

Boonstra, R., Timmer-Bosscha, H., van Echten-Arends, J., van der Kolk, D. M., van den Berg, A., de Jong, B., Tew, K. D., Poppema, S., & de Vries, E. G. E. (2004). Mitoxantrone resistance in a small cell lung cancer cell line is associated with ABCA2 upregulation. *British Journal of Cancer*, *90*(12), 2411–2417. https://doi.org/10.1038/sj.bjc.6601863

Brangi, M., Litman, T., Ciotti, M., Nishiyama, K., Kohlhagen, G., Takimoto, C., Robey, R., Pommier, Y., Fojo, T., & Bates, S. E. (1999). Camptothecin resistance: role of the ATP-binding cassette (ABC), mitoxantrone-resistance half-transporter (MXR), and potential for glucuronidation in MXR-expressing cells. *Cancer Research*, *59*(23), 5938–5946.

Chen, Z.-S., & Tiwari, A. K. (2011). Multidrug resistance proteins (MRPs/ABCCs) in cancer chemotherapy and genetic diseases. *The FEBS Journal*, *278*(18), 3226–3245. https://doi.org/10.1111/j.1742-4658.2011.08235.x

Chiraniya, A., Finkelstein, J., O'Donnell, M., & Bloom, L. B. (2013). A novel function for the conserved glutamate residue in the walker B motif of replication factor C. *Genes*, *4*(2), 134–151. https://doi.org/10.3390/genes4020134

Choi, C.-H. (2005). ABC transporters as multidrug resistance mechanisms and the development of chemosensitizers for their reversal. *Cancer Cell International*, *5*, 30. https://doi.org/10.1186/1475-2867-5-30

Choi, Y. H., & Yu, A.-M. (2014). ABC transporters in multidrug resistance and pharmacokinetics, and strategies for drug development. *Current Pharmaceutical Design*, *20*(5), 793–807. https://doi.org/10.2174/13816128200514021416521 2

Clark, R., Kerr, I. D., & Callaghan, R. (2006). Multiple drugbinding sites on the R482G isoform of the ABCG2 transporter. *British Journal of Pharmacology*, *149*(5), 506–515. https://doi.org/10.1038/sj.bjp.0706904

Cleveland, D. W., Fischer, S. G., & Kirschner andLaemmli, M. W. U. K. (1977). Peptide mapping by limited proteolysis in sodium dodecyl sulfate and analysis by gel electrophoresis. *Journal of Biological Chemistry*, *252*(3), 1102–1106. https://doi.org/10.1016/s0021-9258(19)75212-0

Damiani, D., Tiribelli, M., Geromin, A., Michelutti, A., Cavallin, M., Sperotto, A., & Fanin, R. (2015). ABCG2 overexpression in patients with acute myeloid leukemia: Impact on stem cell transplantation outcome. *American Journal of Hematology*, *90*(9), 784–789. https://doi.org/10.1002/ajh.24084

Dawson, R. J. P., & Locher, K. P. (2006). Structure of a bacterial multidrug ABC transporter. *Nature*, *443*(7108), 180–185. https://doi.org/10.1038/nature05155

Dean, M., Hamon, Y., & Chimini, G. (2001). The human ATP-binding cassette (ABC) transporter superfamily. *Journal of Lipid Research*, *42*(7), 1007–1017.

Doyle, L. A., Yang, W., Abruzzo, L. V, Krogmann, T., Gao, Y., Rishi, A. K., & Ross, D. D. (1998). A multidrug resistance transporter from human MCF-7 breast cancer cells. *Proceedings of the National Academy of Sciences of the United States of America*, *95*(26), 15665–15670. https://doi.org/10.1073/pnas.95.26.15665

Eisenblätter, T., Hüwel, S., & Galla, H.-J. (2003). Characterisation of the brain multidrug resistance protein (BMDP/ABCG2/BCRP) expressed at the blood-brain barrier. *Brain Research*, *971*(2), 221–231. https://doi.org/10.1016/s0006-8993(03)02401-6

Ejendal, K. F. K., Diop, N. K., Schweiger, L. C., & Hrycyna, C. A. (2006). The nature of amino acid 482 of human ABCG2 affects substrate transport and ATP hydrolysis but not substrate binding. *Protein Science : A Publication of the Protein Society*, *15*(7), 1597–1607. https://doi.org/10.1110/ps.051998406

England, C. G., Ehlerding, E. B., & Cai, W. (2016). NanoLuc: A Small Luciferase Is Brightening Up the Field of Bioluminescence. *Bioconjugate Chemistry*, *27*(5), 1175–1187. https://doi.org/10.1021/acs.bioconjchem.6b00112

Ford, R. C., & Beis, K. (2019). Learning the ABCs one at a time: structure and mechanism of ABC transporters. *Biochemical Society Transactions*, *47*(1), 23–36. https://doi.org/10.1042/BST20180147

Frixel, S., Lotz-Havla, A., Kern, S., Kaltenborn, E., Wittmann, T., Gersting, S. W., Muntau, A., Zarbock, R., & Griese, M. (2016). Homooligomerization of ABCA3 and its functional significance. *International Journal of Molecular Medicine*, *38*. https://doi.org/10.3892/ijmm.2016.2650

George, A. M., & Jones, P. M. (2012). Perspectives on the structure–function of ABC transporters: The Switch and Constant Contact Models. *Progress in Biophysics and Molecular Biology*, *109*(3), 95–107. https://doi.org/https://doi.org/10.1016/j.pbiomolbio.2012.06.003

Giacomini, K. M., Huang, S.-M., Tweedie, D. J., Benet, L. Z., Brouwer, K. L. R., Chu, X., Dahlin, A., Evers, R., Fischer, V., Hillgren, K. M., Hoffmaster, K. A., Ishikawa, T., Keppler, D., Kim, R. B., Lee, C. A., Niemi, M., Polli, J. W., Sugiyama, Y., Swaan, P. W., … Zhang, L. (2010). Membrane transporters in drug development. *Nature Reviews. Drug Discovery*, *9*(3), 215–236. https://doi.org/10.1038/nrd3028

Goñi, F. M. (2014). The basic structure and dynamics of cell membranes: An update of the Singer–Nicolson model. *Biochimica et Biophysica Acta (BBA) - Biomembranes*, *1838*(6), 1467–1476. https://doi.org/https://doi.org/10.1016/j.bbamem.2014.01.006

Goulding, J., Mistry, S. J., Soave, M., Woolard, J., Briddon, S. J., White, C. W., Kellam, B., & Hill, S. J. (2021). Subtype selective fluorescent ligands based on ICI 118,551 to study the human β2-adrenoceptor in CRISPR/Cas9 genome-edited HEK293T cells at low expression levels. *Pharmacology Research & Perspectives*, *9*(3), e00779. https://doi.org/10.1002/prp2.779

Graham, F. L., & van der Eb, A. J. (1973). A new technique for the assay of infectivity of human adenovirus 5 DNA. *Virology*, *52*(2), 456–467. https://doi.org/10.1016/0042-6822(73)90341-3

Gulati, S., Jamshad, M., Knowles, T. J., Morrison, K. A., Downing, R., Cant, N., Collins, R., Koenderink, J. B., Ford, R. C., Overduin, M., Kerr, I. D., Dafforn, T. R., & Rothnie, A. J. (2014). Detergent-free purification of ABC (ATP-binding-cassette) transporters. *Biochemical Journal*, *461*(2), 269–278. https://doi.org/10.1042/BJ20131477

Gupta, A., Dai, Y., Vethanayagam, R. R., Hebert, M. F., Thummel, K. E., Unadkat, J. D., Ross, D. D., & Mao, Q. (2006). Cyclosporin A, tacrolimus and sirolimus are potent inhibitors of the human breast cancer resistance protein (ABCG2) and reverse resistance to mitoxantrone and topotecan. *Cancer Chemotherapy and Pharmacology*, *58*(3), 374–383. https://doi.org/10.1007/s00280-005-0173-6

Gupta, A., Zhang, Y., Unadkat, J. D., & Mao, Q. (2004). HIV protease inhibitors are inhibitors but not

substrates of the human breast cancer resistance protein (BCRP/ABCG2). *The Journal of Pharmacology and Experimental Therapeutics*, *310*(1), 334–341. https://doi.org/10.1124/jpet.104.065342

Hankins, H. M., Baldridge, R. D., Xu, P., & Graham, T. R. (2015). Role of flippases, scramblases and transfer proteins in phosphatidylserine subcellular distribution. *Traffic (Copenhagen, Denmark)*, *16*(1), 35–47. https://doi.org/10.1111/tra.12233

Hanson, P. I., & Whiteheart, S. W. (2005). AAA+ proteins: have engine, will work. *Nature Reviews. Molecular Cell Biology*, *6*(7), 519–529. https://doi.org/10.1038/nrm1684

Hediger, M. A., Clémençon, B., Burrier, R. E., & Bruford, E. A. (2013). The ABCs of membrane transporters in health and disease (SLC series): Introduction. *Molecular Aspects of Medicine*, *34*(2), 95–107. https://doi.org/https://doi.org/10.1016/j.mam.2012.12.009

Higgins, C. F., & Linton, K. J. (2004). The ATP switch model for ABC transporters. *Nature Structural & Molecular Biology*, *11*(10), 918–926. https://doi.org/10.1038/nsmb836

Houghton, P. J., Germain, G. S., Harwood, F. C., Schuetz, J. D., Stewart, C. F., Buchdunger, E., & Traxler, P. (2004). Imatinib mesylate is a potent inhibitor of the ABCG2 (BCRP) transporter and reverses resistance to topotecan and SN-38 in vitro. *Cancer Research*, *64*(7), 2333–2337. https://doi.org/10.1158/0008-5472.can-03-3344

Hyde, S. C., Emsley, P., Hartshorn, M. J., Mimmack, M. M., Gileadi, U., Pearce, S. R., Gallagher, M. P., Gill, D. R., Hubbard, R. E., & Higgins, C. F. (1990). Structural model of ATP-binding proteins associated with cystic fibrosis, multidrug resistance and bacterial transport. *Nature*, *346*(6282), 362–365. https://doi.org/10.1038/346362a0

Imai, Y., Asada, S., Tsukahara, S., Ishikawa, E., Tsuruo, T., & Sugimoto, Y. (2003). Breast cancer resistance protein exports sulfated estrogens but not free estrogens. *Molecular Pharmacology*, *64*(3), 610–618. https://doi.org/10.1124/mol.64.3.610

Jackson, S. M., Manolaridis, I., Kowal, J., Zechner, M., Taylor, N. M. I., Bause, M., Bauer, S., Bartholomaeus, R., Bernhardt, G., Koenig, B., Buschauer, A., Stahlberg, H., Altmann, K.-H., & Locher, K. P. (2018). Structural basis of small-molecule inhibition of human multidrug transporter ABCG2. *Nature Structural & Molecular Biology*, *25*(4), 333–340. https://doi.org/10.1038/s41594-018-0049-1

Januchowski, R., Zawierucha, P., Andrzejewska, M., Ruciński, M., & Zabel, M. (2013). Microarray-based detection and expression analysis of ABC and SLC transporters in drug-resistant ovarian cancer cell lines. *Biomedicine & Pharmacotherapy*, *67*(3), 240–245. https://doi.org/https://doi.org/10.1016/j.biopha.2012.11.011

Jones, G. A., & Bradshaw, D. S. (2019). Resonance Energy Transfer: From Fundamental Theory to Recent Applications. *Frontiers in Physics*, *7*, 100. https://doi.org/10.3389/fphy.2019.00100

Jones, P. M., & George, A. M. (2009). Opening of the ADP-bound active site in the ABC transporter ATPase dimer: Evidence for a constant contact, alternating sites model for the catalytic cycle. *Proteins: Structure, Function, and Bioinformatics*, *75*(2), 387–396. https://doi.org/https://doi.org/10.1002/prot.22250

Jonker, J. W., Buitelaar, M., Wagenaar, E., van der Valk, M. A., Scheffer, G. L., Scheper, R. J., Plösch, T., Kuipers, F., Elferink, R. P. J. O., Rosing, H., Beijnen, J. H., & Schinkel, A. H. (2002). The breast cancer resistance protein protects against a major chlorophyll-derived dietary phototoxin and protoporphyria. *Proceedings of the National Academy of Sciences*, *99*(24), 15649–15654. https://doi.org/10.1073/pnas.202607599

Juliano, R. L., & Ling, V. (1976). A surface glycoprotein modulating drug permeability in Chinese hamster ovary cell mutants. *Biochimica et Biophysica Acta*, *455*(1), 152–162. https://doi.org/10.1016/0005-2736(76)90160-7

Kathawala, R. J., Gupta, P., Ashby, C. R., & Chen, Z.-S. (2015). The modulation of ABC transporter-mediated multidrug resistance in cancer: A review of the past decade. *Drug Resistance Updates*, *18*, 1–17. https://doi.org/https://doi.org/10.1016/j.drup.2014.11.002

Kemp, S., Pujol, A., Waterham, H. R., van Geel, B. M., Boehm, C. D., Raymond, G. V, Cutting, G. R., Wanders, R. J., & Moser, H. W. (2001). ABCD1 mutations and the X-linked adrenoleukodystrophy mutation database: role in diagnosis and clinical correlations. *Human Mutation*, *18*(6), 499–515. https://doi.org/10.1002/humu.1227

Kobayashi, H., Picard, L. P., Schönegge, A. M., & Bouvier, M. (2019). Bioluminescence resonance energy transfer–based imaging of protein–protein interactions in living cells. *Nature Protocols*, *14*(4), 1084–1107. https://doi.org/10.1038/s41596-019-0129-7

Krizkova, V., Dubova, M., Susova, S., Vycital, O., Bruha, J., Skala, M., Liska, V., Daum, O., & Soucek, P. (2016). Protein expression of ATP-binding cassette transporters ABCC10 and ABCC11 associates with survival of colorectal cancer patients. *Cancer Chemotherapy and Pharmacology*, *78*(3), 595–603. https://doi.org/10.1007/s00280-016-3114-7

Lagas, J. S., van der Kruijssen, C. M. M., van de Wetering, K., Beijnen, J. H., & Schinkel, A. H. (2009). Transport of diclofenac by breast cancer resistance protein (ABCG2) and stimulation of multidrug resistance protein 2 (ABCC2)-mediated drug transport by diclofenac and benzbromarone. *Drug Metabolism and Disposition: The Biological Fate of Chemicals*, *37*(1), 129–136. https://doi.org/10.1124/dmd.108.023200

Laurens, C., Abot, A., Delarue, A., & Knauf, C. (2019). Central Effects of Beta-Blockers May Be Due to Nitric Oxide and Hydrogen Peroxide Release Independently of Their Ability to Cross the Blood-Brain Barrier. *Frontiers in Neuroscience*, *13*. https://doi.org/10.3389/fnins.2019.00033

Lebkowski, J. S., Clancy, S., & Calos, M. P. (1985). Simian virus 40 replication in adenovirus-transformed human cells antagonizes gene expression. *Nature*, *317*(6033), 169–171. https://doi.org/10.1038/317169a0

Lee, J.-Y., Kinch, L. N., Borek, D. M., Wang, J., Wang, J., Urbatsch, I. L., Xie, X.-S., Grishin, N. V, Cohen, J. C., Otwinowski, Z., Hobbs, H. H., & Rosenbaum, D. M. (2016). Crystal structure of the human sterol transporter ABCG5/ABCG8. *Nature*, *533*(7604), 561–564. https://doi.org/10.1038/nature17666

Li, S., Sjögren, H. O., Hellman, U., Pettersson, R. F., & Wang, P. (1997). Cloning and functional characterization of a subunit of the transporter associated with antigen processing. *Proceedings of the National Academy of Sciences of the United States of America*, *94*(16), 8708–8713. https://doi.org/10.1073/pnas.94.16.8708

Lin, L., Yee, S. W., Kim, R. B., & Giacomini, K. M. (2015). SLC transporters as therapeutic targets: emerging opportunities. *Nature Reviews. Drug Discovery*, *14*(8), 543–560. https://doi.org/10.1038/nrd4626

Mairinger, S., Zoufal, V., Wanek, T., Traxl, A., Filip, T., Sauberer, M., Stanek, J., Kuntner, C., Pahnke, J., Müller, M., & Langer, O. (2018). Influence of breast cancer resistance protein and P-glycoprotein on tissue distribution and excretion of Ko143 assessed with PET imaging in mice. *European Journal of Pharmaceutical Sciences : Official Journal of the European Federation for Pharmaceutical Sciences*, *115*, 212–222. https://doi.org/10.1016/j.ejps.2018.01.034

Martin, C., Berridge, G., Mistry, P., Higgins, C., Charlton, P., & Callaghan, R. (1999). The molecular interaction of the high affinity reversal agent XR9576 with P-glycoprotein. *British Journal of Pharmacology*, *128*(2), 403–411. https://doi.org/10.1038/sj.bjp.0702807

Marzac, C., Garrido, E., Tang, R., Fava, F., Hirsch, P., De Benedictis, C., Corre, E., Lapusan, S., Lallemand, J.-Y., Marie, J.-P., Jacquet, E., & Legrand, O. (2011). ATP Binding Cassette transporters associated with chemoresistance: transcriptional profiling in extreme cohorts and their prognostic impact in a cohort of 281 acute myeloid leukemia patients. *Haematologica*, *96*(9), 1293–1301. https://doi.org/10.3324/haematol.2010.031823

McDevitt, C. A., Collins, R., Kerr, I. D., & Callaghan, R. (2009). Purification and structural analyses of ABCG2. *Advanced Drug Delivery Reviews*, *61*(1), 57–65. https://doi.org/https://doi.org/10.1016/j.addr.2008.07.004

McDevitt, C. A., Crowley, E., Hobbs, G., Starr, K. J., Kerr, I. D., & Callaghan, R. (2008). Is ATP binding responsible for initiating drug translocation by the multidrug transporter ABCG2? *The FEBS Journal*, *275*(17), 4354–4362. https://doi.org/https://doi.org/10.1111/j.1742-4658.2008.06578.x

Miyake, K., Mickley, L., Litman, T., Zhan, Z., Robey, R., Cristensen, B., Brangi, M., Greenberger, L., Dean, M., Fojo, T., & Bates, S. E. (1999). Molecular cloning of cDNAs which are highly overexpressed in mitoxantrone-resistant cells: demonstration of homology to ABC transport genes. *Cancer Research*, *59*(1), 8–13.

Mo, W., & Zhang, J.-T. (2012). Human ABCG2: structure, function, and its role in multidrug resistance. *International Journal of Biochemistry and Molecular Biology*, *3*(1), 1–27.

Namkung, Y., Le Gouill, C., Lukashova, V., Kobayashi, H., Hogue, M., Khoury, E., Song, M., Bouvier, M., & Laporte, S. A. (2016). Monitoring G protein-coupled receptor and β-arrestin trafficking in live cells using enhanced bystander BRET. *Nature Communications*, *7*(1), 12178. https://doi.org/10.1038/ncomms12178

Ni, Z., Bikadi, Z., Rosenberg, M. F., & Mao, Q. (2010). Structure and function of the human breast cancer resistance protein (BCRP/ABCG2). *Current Drug Metabolism*, *11*(7), 603–617. https://doi.org/10.2174/138920010792927325

Ni, Z., Mark, M. E., Cai, X., & Mao, Q. (2010). Fluorescence resonance energy transfer (FRET) analysis demonstrates dimer/oligomer formation of the human breast cancer resistance protein (BCRP/ABCG2) in intact cells. *International Journal of Biochemistry and Molecular Biology*, *1*(1), 1–11.

Olejko, L., & Bald, I. (2017). FRET efficiency and antenna effect in multi-color DNA origami-based light harvesting systems. *RSC Adv.*, *7*(39), 23924–23934. https://doi.org/10.1039/C7RA02114C

Omote, H., Hiasa, M., Matsumoto, T., Otsuka, M., & Moriyama, Y. (2006). The MATE proteins as fundamental transporters of metabolic and xenobiotic organic cations. *Trends in Pharmacological Sciences*, *27*(11), 587–593. https://doi.org/10.1016/j.tips.2006.09.001

Pan, G., Giri, N., & Elmquist, W. F. (2007). Abcg2/Bcrp1 mediates the polarized transport of antiretroviral nucleosides abacavir and zidovudine. *Drug Metabolism and Disposition: The Biological Fate of Chemicals*, *35*(7), 1165–1173. https://doi.org/10.1124/dmd.106.014274

Pozza, A., Perez-Victoria, J. M., Sardo, A., Ahmed-Belkacem, A., & Di Pietro, A. (2006). Purification of breast cancer resistance protein ABCG2 and role of arginine-482. *Cellular and Molecular Life Sciences : CMLS*, *63*(16), 1912–1922. https://doi.org/10.1007/s00018-006-6159-7

Qian, H., Zhao, X., Cao, P., Lei, J., Yan, N., & Gong, X. (2017). Structure of the Human Lipid Exporter ABCA1. *Cell*, *169*(7), 1228-1239.e10. https://doi.org/10.1016/j.cell.2017.05.020

Qin, Y., Dongchun, N., Julia, K., Ioannis, M., Scott M., J., Henning, S., & Kaspar P., L. (2021). Structures of ABCG2 under turnover conditions reveal a key step in drug transport mechanism. *BioRxiv*, *45*, 2021.03.03.433600. https://doi.org/10.1038/s41467-021-24651-2

Rabindran, S. K., He, H., Singh, M., Brown, E., Collins, K. I., Annable, T., & Greenberger, L. M. (1998). Reversal of a Novel Multidrug Resistance Mechanism in Human Colon Carcinoma Cells by Fumitremorgin C. *Cancer Research*, *58*(24), 5850. http://cancerres.aacrjournals.org/content/58/24/5850.abstract

Rath, A., Glibowicka, M., Nadeau, V. G., Chen, G., & Deber, C. M. (2009). Detergent binding explains anomalous SDS-PAGE migration of membrane proteins. *Proceedings of the National Academy of Sciences of the United States of America*, *106*(6), 1760–1765. https://doi.org/10.1073/pnas.0813167106

Robey, R. W., To, K. K. K., Polgar, O., Dohse, M., Fetsch, P., Dean, M., & Bates, S. E. (2009). ABCG2: a perspective. *Advanced Drug Delivery Reviews*, *61*(1), 3–13. https://doi.org/10.1016/j.addr.2008.11.003

Schmitz, G., & Langmann, T. (2001). Structure, function and regulation of the ABC1 gene product. *Current Opinion in Lipidology*, *12*(2). https://journals.lww.com/co-lipidology/Fulltext/2001/04000/Structure,_function_and_regulation_of_the_ABC1.6.aspx

Sheppard, D. N., & Welsh, M. J. (1999). Structure and function of the CFTR chloride channel. *Physiological Reviews*, *79*(1 Suppl), S23-45. https://doi.org/10.1152/physrev.1999.79.1.S23

Shukla, S., Robey, R. W., Bates, S. E., & Ambudkar, S. V. (2005). Dihydropyridines, nicardipine, nifedipine and reserpine modulate the function of multidrug resistance-linked ABCG2 transporter. *Cancer Research*, *65*(9 Supplement), 121. http://cancerres.aacrjournals.org/content/65/9_Supplement/121.3.abstract

Singer, S. J., & Nicolson, G. L. (1972). The fluid mosaic model of the structure of cell membranes. *Science (New York, N.Y.)*, *175*(4023), 720–731. https://doi.org/10.1126/science.175.4023.720

Stoddart, L. A., Johnstone, E. K. M., Wheal, A. J., Goulding, J., Robers, M. B., Machleidt, T., Wood, K. V, Hill, S. J., & Pfleger, K. D. G. (2015). Application of BRET to monitor ligand binding to GPCRs. *Nature Methods*, *12*(7), 661–663. https://doi.org/10.1038/nmeth.3398

Stoddart, L. A., Kilpatrick, L. E., & Hill, S. J. (2018). NanoBRET Approaches to Study Ligand Binding to GPCRs and RTKs. *Trends in Pharmacological Sciences*, *39*(2), 136–147. https://doi.org/https://doi.org/10.1016/j.tips.2017.10.006

Taylor, N. M. I., Manolaridis, I., Jackson, S. M., Kowal, J., Stahlberg, H., & Locher, K. P. (2017). Structure of the human multidrug transporter ABCG2. *Nature*, *546*(7659), 504–509.

https://doi.org/10.1038/nature22345

Theodoulou, F. L., & Kerr, I. D. (2015). ABC transporter research: going strong 40 years on. *Biochemical Society Transactions*, *43*(5), 1033–1040. https://doi.org/10.1042/BST20150139

Toyoda, Y., Takada, T., & Suzuki, H. (2019). Inhibitors of Human ABCG2: From Technical Background to Recent Updates With Clinical Implications. *Frontiers in Pharmacology*, *10*, 208. https://doi.org/10.3389/fphar.2019.00208

Vaidyanathan, A., Sawers, L., Gannon, A.-L., Chakravarty, P., Scott, A. L., Bray, S. E., Ferguson, M. J., & Smith, G. (2016). ABCB1 (MDR1) induction defines a common resistance mechanism in paclitaxel- and olaparib-resistant ovarian cancer cells. *British Journal of Cancer*, *115*(4), 431–441. https://doi.org/10.1038/bjc.2016.203

van Herwaarden, A. E., Wagenaar, E., Merino, G., Jonker, J. W., Rosing, H., Beijnen, J. H., & Schinkel, A. H. (2007). Multidrug transporter ABCG2/breast cancer resistance protein secretes riboflavin (vitamin B2) into milk. *Molecular and Cellular Biology*, *27*(4), 1247–1253. https://doi.org/10.1128/MCB.01621-06

Vasiliou, V., Vasiliou, K., & Nebert, D. W. (2009). *Human ATP-binding cassette (ABC) transporter family*. *3*(3), 281–290.

Volk, E. L., & Schneider, E. (2003). Wild-type breast cancer resistance protein (BCRP/ABCG2) is a methotrexate polyglutamate transporter. *Cancer Research*, *63*(17), 5538–5543.

Walker, J. E., Saraste, M., Runswick, M. J., & Gay, N. J. (1982). Distantly related sequences in the alpha- and beta-subunits of ATP synthase, myosin, kinases and other ATP-requiring enzymes and a common nucleotide binding fold. *The EMBO Journal*, *1*(8), 945–951.

Weidner, L. D., Zoghbi, S. S., Lu, S., Shukla, S., Ambudkar, S. V, Pike, V. W., Mulder, J., Gottesman, M. M., Innis, R. B., & Hall, M. D. (2015). The Inhibitor Ko143 Is Not Specific for ABCG2. *The Journal of Pharmacology and Experimental Therapeutics*, *354*(3), 384–393. https://doi.org/10.1124/jpet.115.225482

Wilkens, S. (2015). Structure and mechanism of ABC transporters. *F1000prime Reports*, *7*, 14. https://doi.org/10.12703/P7-14

Wong, K., Briddon, S. J., Holliday, N. D., & Kerr, I. D. (2016). Plasma membrane dynamics and tetrameric organisation of ABCG2 transporters in mammalian cells revealed by single particle imaging techniques. *Biochimica et Biophysica Acta - Molecular Cell Research*, *1863*(1), 19–29. https://doi.org/10.1016/j.bbamcr.2015.10.002

Woodward, O. M., Tukaye, D. N., Cui, J., Greenwell, P., Constantoulakis, L. M., Parker, B. S., Rao, A.,

Köttgen, M., Maloney, P. C., & Guggino, W. B. (2013). Gout-causing Q141K mutation in ABCG2 leads to instability of the nucleotide-binding domain and can be corrected with small molecules. *Proceedings of the National Academy of Sciences*, *110*(13), 5223 LP – 5228. https://doi.org/10.1073/pnas.1214530110

Wrigley, R., Phipps-Green, A. J., Topless, R. K., Major, T. J., Cadzow, M., Riches, P., Tausche, A.-K., Janssen, M., Joosten, L. A. B., Jansen, T. L., So, A., Harré Hindmarsh, J., Stamp, L. K., Dalbeth, N., & Merriman, T. R. (2020). Pleiotropic effect of the ABCG2 gene in gout: involvement in serum urate levels and progression from hyperuricemia to gout. *Arthritis Research & Therapy*, *22*(1), 45. https://doi.org/10.1186/s13075-020-2136-z

Xiao, Y., Davidson, R., Smith, A., Pereira, D., Zhao, S., Soglia, J., Gebhard, D., de Morais, S., & Duignan, D. B. (2006). A 96-Well Efflux Assay To Identify ABCG2 Substrates Using a Stably Transfected MDCK II Cell Line. *Molecular Pharmaceutics*, *3*(1), 45–54. https://doi.org/10.1021/mp050088t

Xiong, H., Callaghan, D., Jones, A., Bai, J., Rasquinha, I., Smith, C., Pei, K., Walker, D., Lue, L.-F., Stanimirovic, D., & Zhang, W. (2009). ABCG2 is upregulated in Alzheimer's brain with cerebral amyloid angiopathy and may act as a gatekeeper at the blood-brain barrier for Abeta(1-40) peptides. *The Journal of Neuroscience : The Official Journal of the Society for Neuroscience*, *29*(17), 5463–5475. https://doi.org/10.1523/JNEUROSCI.5103-08.2009

Yang, C. H., Schneider, E., Kuo, M. L., Volk, E. L., Rocchi, E., & Chen, Y. C. (2000). BCRP/MXR/ABCP expression in topotecan-resistant human breast carcinoma cells. *Biochemical Pharmacology*, *60*(6), 831–837. https://doi.org/10.1016/s0006-2952(00)00396-8

Yu, X.-H., Qian, K., Jiang, N., Zheng, X.-L., Cayabyab, F. S., & Tang, C.-K. (2014). ABCG5/ABCG8 in cholesterol excretion and atherosclerosis. *Clinica Chimica Acta; International Journal of Clinical Chemistry*, *428*, 82–88. https://doi.org/10.1016/j.cca.2013.11.010

Zhang, Y., Bressler, J. P., Neal, J., Lal, B., Bhang, H.-E. C., Laterra, J., & Pomper, M. G. (2007). ABCG2/BCRP Expression Modulates d-Luciferin{\textendash}Based Bioluminescence Imaging. *Cancer Research*, *67*(19), 9389–9397. https://doi.org/10.1158/0008-5472.CAN-07-0944

Zhu, X., Zhang, H., & Mendell, J. T. (2020). Ribosome Recycling by ABCE1 Links Lysosomal Function and Iron Homeostasis to 3' UTR-Directed Regulation and Nonsense-Mediated Decay. *Cell Reports*, *32*(2), 107895. https://doi.org/https://doi.org/10.1016/j.celrep.2020.107895